Extensive longevity and DNA virus-driven adaptation in nearctic Myotis bats

Juan M Vazquez[1†], M. Elise Lauterbur[2,3†], Saba Mottaghinia[4], Melanie Bucci[2], Devaughn Fraser[5,6], Genavieve Gray-Sandoval[2], Léa Gaucherand[7], Zeinab R Haidar[8,9], Melissa Han[10], William Kohler[10], Tanya M. Lama[11], Amandine Le Corf[4], Sarah Maesen[4], Dakota McMillan[1,12], Stacy Li[1,13], Johnathan Lo[13], Carine Rey[4], Samantha LR Capel[6], Michael Singer[14], Kathleen Slocum[15], William Thomas[16], Janet Debelak Tyburec[17], Sarah Villa[14], Richard Miller[10], Michael Buchalski[5], Jose Pablo Vazquez-Medina[1], Sébastien Pfeffer[7], Lucie Etienne[4]***, David Enard[2‡]**, Peter H Sudmant[1,13‡]*

Affiliations:

1. Department of Integrative Biology, University of California, Berkeley, Berkeley, CA USA
2. Department of Ecology and Evolutionary Biology, University of Arizona, Tucson, AZ USA
3. Current affiliation: Department of Biology, University of Vermont, Burlington, VT USA
4. Centre International de Recherche en Infectiologie (CIRI), Inserm U1111, UCBL1, CNRS UMR5308, Ecole Normale Supérieure ENS de Lyon, Université de Lyon, Lyon, France
5. Wildlife Genetics Research Unit, Wildlife Health Laboratory, California Department of Fish and Wildlife, Sacramento, CA, United States
6. Current affiliation: Wildlife Diversity Program, Wildlife Division, Connecticut Department of Energy and Environmental Protection, Burlington, CT, United States
7. Université de Strasbourg, Architecture et Réactivité de l'ARN, Institut de Biologie Moléculaire et Cellulaire du CNRS, Strasbourg, France.
8. Department of Biology, California State Polytechnic University, Humboldt, Arcata, CA USA
9. Current affiliation: Western EcoSystems Technology Inc, Cheyenne, WY USA
10. Department of Pathology and Clinical Laboratories, University of Michigan, Ann Arbor, MI USA
11. Department of Biological Sciences, Smith College, Northampton, MA USA
12. Department of Science and Biotechnology, Berkeley City College, Berkeley, CA USA
13. Center for Computational Biology, University of California, Berkeley, Berkeley, CA USA
14. Department of Molecular and Cellular Biology, University of California, Berkeley, Berkeley, CA USA
15. Bat Conservation International, Austin, TX USA
16. Department of Ecology and Evolution, Stony Brook University, Stony Brook NY USA
17. Bat Survey Solutions, LLC, Tucson, AZ USA

† Contributed equally as first authors
‡ Contributed equally as senior authors

* Correspondence: psudmant@berkeley.edu
** Correspondence: denard@arizona.edu
*** Correspondence: lucie.etienne@ens-lyon.fr

Keywords: Aging, Bats, Cancer, Evolutionary Biology, Functional Genomics, Immunity, Infectious Disease

Abstract

The rich species diversity of bats encompasses extraordinary adaptations, including extreme longevity and tolerance to infectious disease. While traditional approaches using genetic screens in model organisms have uncovered some fundamental processes underlying these traits, model organisms do not possess the variation required to understand the evolution of traits with complex genetic architectures. In contrast, the advent of genomics at tree-of-life scales enables us to study the genetic interactions underlying these processes by leveraging millions of years of evolutionary trial-and-error. Here, we use the rich species diversity of the genus *Myotis* - one of the longest-living clades of mammals - to study the evolution of longevity-associated traits and infectious disease using functional evolutionary genomics. We generated reference genome assemblies and cell lines for 8 closely-related (~11 MYA) species of *Myotis* rich in phenotypic and life history diversity. Using genome-wide screens of positive selection, analysis of structural variation and copy number variation, and functional experiments in primary cell lines, we identify new patterns of adaptation in longevity, cancer resistance, and viral interactions both within *Myotis* and across bats. We find that the rapid evolution of lifespan in *Myotis* has some of the most significant variations in cancer risk across mammals, and demonstrate a unique DNA damage response in the long-lived *M. lucifugus* using primary cell culture models. Furthermore, we find evidence of abundant adaptation in response to DNA viruses, but not RNA viruses, in *Myotis* and other bats. This is in contrast to these patterns of adaptation in humans, which might contribute to the importance of bats as a reservoir of zoonotic viruses. Together, our results demonstrate the utility of leveraging natural variation to understand the genomics of traits with implications for human health and suggest important pleiotropic relationships between infectious disease tolerance and cancer resistance.

Introduction

Bats (order *Chiroptera*) represent approximately 20% of all known mammalian species and are one of the most phenotypically diverse clades of mammals[1,2]. Since their emergence 60 million years ago[3–5], many bat lineages have independently evolved a wide variety of life history strategies and phenotypic traits, including exceptional changes in longevity, viral tolerance, and immune defense[6–11]. Such systems, in which shared traits have evolved *de novo* multiple times, are powerful resources for dissecting the genetic basis of phenotypes. Rigorous approaches to studying these traits, however, depend on high-quality, well-annotated genomes to test evolutionary and genomic hypotheses, and on experimental functional systems to validate these hypotheses.

The largest genus of bats - *Myotis* - is estimated to have emerged approximately 33 million years ago[12,13], and encompasses over 139 described species spanning six continents and a wide range of ecological niches[1,12–14]. Extraordinary changes in lifespan have independently evolved multiple times in *Myotis*, including the most extreme variation in lifespan amongst mammals[6,15–18]. There exists a six-fold difference in lifespan between the longest-lived species (*M. brandtii*, 42 years[15,19], **Figure 1A**) and the shortest-lived species (*M. nigricans*, 7 yrs[15,20]) which diverged approximately 10.6 million years ago[5,14,21,22]. In addition, *Myotis* species have been used as systems for investigating virus tolerance and other pathogen resistance[23–25] associated with the expansion and contraction of antiviral defenses[26–29], which have contributed to bats' ecological role as zoonotic reservoirs[10,11,30–33].

The origin, evolution, and functional basis of these phenotypes have been studied using two major approaches: comparative evolutionary methods, and model organism-based experimental work. The power of comparative evolutionary studies is constrained by several factors including incomplete phylogenetic coverage;

poor temporal resolution; the quality and composition of gene annotations; and availability of functional data and tools for validation. Rapidly evolving genes, such as those associated with adaptations to pathogens [34–36], present particular challenges for homology and alignment based methods. Similarly, poor phenotypic resolution and long divergence times between study species hinders the power of statistical approaches to identify patterns of selection and diversification[37–40]. Meanwhile, model organism-based approaches contribute a different, complementary perspective and provide the power of functional analyses; however, these studies can suffer from issues related to the suitability and diversity of the model species' genotype and phenotype.

For example, many studies of the genetic basis of vital processes such as longevity are based on short-lived model organisms[41,42]. While these studies have been crucial for identifying and dissecting several key aging pathways, comparative studies of exceptionally long-lived organisms have uncovered novel genes and pleiotropic effects governing lifespan[36,41,43–53]. The comparative approach, however, has historically been hindered by limitations in available genomic resources and genetic tools for study. Similarly, studies of infectious disease response are common and powerful in model organisms, but the lack of diversity and inbred lines limits their scope. Bats in particular present an important case study in, and opportunity to study, variation in virus adaptation strategies due to their role as zoonotic reservoirs and their specific resistance to viruses[36,54]. While previous studies have shown unique infectious disease adaptations in bats, including loss of important inflammatory genes and expansions of and adaptation in some immune gene families[54–56], they are typically hampered by the breadth and number of species analyzed, and only rarely functionally validate results from genomic analyses.

Here we combined comparative and functional approaches in *Myotis* to uncover strong genomic and functional evidence of adaptation to both aging-related and infectious diseases. We present for the first time a robust quantification of relative intrinsic cancer risk across mammals, finding that *Myotis* are overrepresented at the extreme of increased cancer risk. Consistent with this observation, we identified pervasive selection of genes in longevity- and cancer-related processes, especially in lineages which have undergone the greatest changes in lifespan. Furthermore, we found strong evidence of adaptation in response to DNA viruses in Myotis and other bats. Genome-wide enrichment of adaptation being driven by DNA viruses is unique to bats in comparison with other large groups of mammals. Finally, using near-complete assemblies, we identified structural variations encompassing stress response, immunity, and inflammation genes, including a trans-species copy number polymorphism of protein kinase R (PKR). Together, our results suggest that pleiotropy and co-evolution of traits in *Myotis* has played a key role in the evolution of exceptional longevity and infectious disease resistance.

Results

High quality chromosome-level assemblies of 8 *Myotis* bat species

To study how lifespan and viral response have evolved in *Myotis*, we collected skin punches and derived primary cell lines from several North American ("Nearctic")[21] species (**Figure 1A,C),** including one of the longest-lived mammals, *Myotis lucifugus*[15]. Using these cell lines and flash frozen tissues we generated *de novo* haplotype-resolved, chromosome-scale genome assemblies for eight species (**Figure 1A**) using a combination of long-read PacBio HiFi sequencing and HiC scaffolding. These genomes are highly contiguous, with an average of 98.6% of nucleotide content assembled into 22-23 syntenic chromosome-scale scaffolds corresponding to the published karyotype[57] with an average QV of 66. These genomes have among the lowest auNG scores of any *Chiroptera* genome published to date (**Figure 1A, E**; **Table S1**). Across all 8 genomes, each

autosome has been completely assembled telomere-to-telomere (T2T) in at least one species (**Figure 1E**). Within assemblies, 29%-70% of chromosomes are fully assembled with an average of less than one gap per chromosome (**Table S1**). When comparing the assemblies of species generated from tissue samples versus primary cell lines, we found that they were broadly comparable and structurally similar. However, genomes assembled from cell lines had slightly improved statistics likely attributable to the increased quality and molecular weight of extracted DNA (**Figure 1A, D, E; Table S1**).

Genomes were annotated using well-established pipelines[36] leveraging multiple lines of evidence, including short-read RNAseq, gene prediction (AUGUSTUS-CGP[58], GeneMark-ES[59]; gene projections[60], TOGA[61]); and homology (miniprot[62]). In total, we identified an average of 27,536 protein coding genes per species. We benchmarked our annotations using BUSCO[63,64] (V5.4.3) mammalian ortholog sets indicating these annotations are 98.2%-98.5% complete (**Figure 1C**). We also annotated a recent assembly of *Myotis yumanensis*[65] for inclusion in downstream analyses. Overall, these fully annotated genomes represent some of the most contiguous *Laurasiatheria* assemblies to date.

Resolving the phylogeny and the evolution of body size and lifespan in nearctic *Myotis*

The phylogenetic relationships within *Myotis* have been the subject of much debate, with a number of conflicting phylogenies described in the literature based on different choices of genetic markers[14,66–69]. To resolve the phylogeny of Nearctic *Myotis*, we identified single copy orthologs of 17,509 protein genes present in at least 4 of our 536 mammalian genomes using *miniprot*[62] and the SwissProt database[70], resulting in 30.6M aligned nucleotides. These alignments were used to build a maximum likelihood tree of *Eutheria*. The *Chiroptera* sub-clade was then time-calibrated using *mcmctree*[71,72] and available fossil-based node calibrations (**Figure 1B**; **Figure S1**; **Table S2**). Our results conclusively recapitulate known sister species pairs including *M. lucifugus* and *M. occultus*; *M. yumansis and M. velifer*; and *M. evotis* and *M. thysanodes*. Our proposed phylogeny resolves the complex relationship between these sister taxa, with 100% bootstrap support at all nodes throughout *Chiroptera*.

Using our resolved Nearctic *Myotis* phylogeny, we re-examined the evolution of body size and lifespan in *Chiroptera*. In mammals and other metazoans, there is a strong allometric scaling (positive correlation with body size) of lifespan. Bats have been noted as an exception to this rule: they are exceptionally long-lived for their body size[17,18,73], and this exceptional longevity has evolved *de novo* multiple times[6,73,74]. However, these observations have not been tested using phylogenetically corrected statistics, leveraging well-resolved phylogenies. To test the hypothesis of non-allometric scaling of lifespan in bats, we modeled the evolution of body size and lifespan across a supertree of over 1000 placental mammals (*Eutheria*)[67] (**Figure 2**; **Table S2**). In agreement with previous studies in vertebrates[7,17,46,51,75–83], changes in body size are pervasive across mammals, with extreme changes seen in whales (*Cetacea*)[81,82], elephantids (*Proboscidea*)[44,46,75], and in sloths and armadillos (*Xenarthra*)[76,83–85]. Within bats, major changes in body size are only observed at the root of the lineage and within *Yinpterochrioptera* (megabats including genera *Pteropus, Eidolon, Megaderma,* and *Rhinolophus*). Outside of these clades, only minor changes in body size were observed (**Figure 2A**). The evolution of lifespan across mammals mirrors the evolution of body size, with additional variability. Branches with large increases in body size (e.g. *Cetacea* ancestor, *Primate* ancestor) have also experienced large increases in lifespan (**Figure 2B)**, leading to an overall positive association between lifespan and body size (**Figure S2A**). However, despite little change in body size in bats (**Figure 2A, C**), we observed some of the largest changes in lifespan across

mammals towards the tips of the tree (**Figure 2B, D**), consistent with the theory of multiple independent increases in lifespan across bats. This is especially true in *Myotis*, where we saw many of the fastest increases in lifespan, including for *Myotis grisescens* (4.15x increase, 100th percentile), *Myotis brandtii* (2.25x increase, 100th percentile), *Myotis lucifugus* (1.56x, 98th percentile), *Myotis myotis* (1.1x increase, 79nd percentile), and the *Myotis* common ancestor (1.26x increase, 92rd percentile) (**Figure 2D; Figure S2C; Table S2**). We next used phylogenetically-corrected generalized linear models and ANCOVA to study the relationship between body size and lifespan across mammals. While we find that non-bat mammals experience a 0.159% increase in lifespan per 1% increase in body size, bats experience a 0.223% increase in lifespan years per 1% increase in body size; these rates were not significantly different, however, suggesting that lifespan allometry is conserved in bats after accounting for phylogeny (**Figure S2E-F**; pANCOVA, p=0.29).

Rapid changes in body size and lifespan can have major implications for the evolution of cancer risk and resistance across mammals. The lifetime cancer risk of an individual is modeled as the product of body size (i.e. the number of cells within an individual), lifespan, and a constant representing the intrinsic cancer risk per cell and unit time. Within species, lifetime cancer risk scales linearly with body size, and with lifespan by a power-law of exponent 6[86–89]. In contrast to this within-species relationship, there is no significant correlation between these traits across species[89–92] - a phenomenon known as Peto's Paradox. The observation of similar lifetime cancer incidence rates across mammals[76,92,93] implies that species possess distinct intrinsic cancer risks per cell to compensate for changes in lifespan and/or body size. Thus, large bodied, long lived mammals must evolve increased *cancer resistance* proportional to their increased *cancer risk* to avoid increased rates of cancer and death (**Figure 2E**).

We thus hypothesized that the very rapid evolution of increased lifespan in *Myotis* would result in a dramatic increase in their expected cancer risk compared to other mammals. Given consistent cancer rates across mammalian clades[76,92,93], the Reduced Intrinsic Cancer Risk per cell (RICR) between an extant mammal and its most recent ancestor can be calculated as the log ratio of body size and lifespan between the two nodes (**Figure 2E**)[46,89]. We thus used our estimates of body size and lifespan across *Eutheria* to quantify changes in (RICR) across placental mammals (**Figure 2F**)[46]. We found that bats were slightly overrepresented at the top 10% of RICR, with an odds ratio of 1.15 at the highest extreme, highlighting the impact of rapid lifespan evolution on cancer risk. Importantly, the longest-lived *Myotis* (*M. grisescens*, 39 yrs & 1st pct; *M. brandtii*, 42 yrs & 2nd percentile; *M. lucifugus*, 36 yrs & 4th pct) and their most recent common ancestors (*lucifugus-occultus*, ~26 yrs & 8th pct; *Myotis* common ancestor, ~22 yrs & 14th pct) demonstrated some of the most pronounced decreases in RICR among mammals (**Figure 2F; Figure S2D; Table S2**). Similar to other extreme cases of body size and lifespan in vertebrates[46,48,51,53,76,94–97], the pronounced changes in RICR seen in *Myotis* imply an extraordinarily strong selective pressure to evolve cancer resistance mechanisms at multiple points across *Chiroptera* in general, and within *Myotis* in particular.

Evolutionary signatures of cancer resistance in *Myotis*

We next set out to identify genes under positive selection across our phylogeny of Nearctic *Myotis*. We used aBSREL[98] to test for branch-specific positive selection among 15,734 single-copy orthologous genes identified in at least 4 of our 536 mammalian genomes. We found that on average, 22.7% of genes were under selection across the 9 nearctic *Myotis* species and their internal branches after multiple testing correction at FDR<=5%; and 5.23% of genes were significant and had omega values above 1, signaling positive selection (**Table S3**). These genes were enriched for several pathways involved in immunity, cancer, and aging (**Table S3**). Many of these genes lie at the intersection of these two processes, including members of the Cluster of

Differentiation (CD) family, Serpin family, insulin signaling pathway, redox repair, and iron storage (**Figure 3A; Table S3**), suggesting possible pleiotropic influences on genes under selection.

To test this, we quantified the contribution of genes under selection to pathways associated with the hallmark of cancer[99–101] by measuring the proportion of cancer-associated pathways overrepresented among genes under selection throughout the phylogeny (**Figure 3A; insets**). Many nodes within nearctic *Myotis* were enriched for cancer hallmark pathways, especially at the recent ancestors of the longest-lived species (e.g. *M. lucifugus, M. occultus*; **Figure 3A**). Testing the overall contribution of genes that have undergone selection in each species since the common *Myotis* ancestor, we observed significant enrichments in the representation of cancer-associated pathways only in species lineages with reductions in RICR (*M. lucifugus*, *M. occultus, M. evotis, M. thysanodes, M. yumanensis;* **Figure 3B**). This suggests that while genes under selection in nearctic *Myotis* frequently contribute to cancer-associated pathways, cancer resistance has only driven consistent selection in the longest-lived lineages with the greatest increases in cancer risk.

We also observed that many key genes involved in ferroptosis - specifically in iron transport, glutathione metabolism, and lipid peroxidation - were under selection at multiple instances throughout the phylogeny (**Table S3**). Many of these genes were recurrently under selection in each species' lineage, such as with ferritin (both heavy and light chains) at three distinct points in the evolutionary history of *M. yumanensis*. Genes under selection in iron transport are specifically involved in the regulation of free iron in the cell, specifically in the export & reduction of the free radical catalyst Fe^{2+} (ferroportin, *HMOX1*) and the import, storage, and maintenance of Fe^{3+} (ferritin and transferrin receptors 1 and 2). Additionally, we observe selective signatures in glutathione metabolism and oxidative stress response including: *SLC3A2* and *SLC7A11*, a heterodimer pair facilitating cystine import and glutamate export; glutathione synthetase; and glutathione peroxidase 3 (*GPX3*). Finally, we observed a pattern of selection in genes involved in synthesizing and maintaining key polyunsaturated fatty acids involved in ferroptosis, including *LPCAT3*, *ALOX15*, and *PRDX5*.

To test for intensified and relaxed selection in genes in long-lived or short-lived *Myotis*, we ran RELAX[102] on 12,438 genes present across 11 *Myotis* species, identifying 263 genes under intensified selection ($k>1$) and 101 genes under relaxed selection ($k\leq1$) after multiple testing correction ($p_{adj}\leq0.05$). Among genes of note showing significant intensified selection were *USP9X* (an X-linked ubiquitin protease associated with cancer and T cell development[103,104], $k=48.6$); *CDK16* (an oncogenic cyclin-dependent kinase that regulates autophagy[105,106], $k=44.9$); and *FGFR2* (a cell growth receptor associated with human cancers that is also a VIP[107,108], $k=26.1$) (**Figure S3B; Table S4)**. Performing a gene set enrichment analysis for the 364 significant genes, we find a strong association among selected genes with FGF2 signaling, chromatin remodeling, and pathways associated with both retroviruses and coronaviruses, further highlighting the pleiotrophic nature of selection patterns in *Myotis* (**Figure S3C; Table S4**). Finally, using RERConverge[109], we investigated how genes' evolutionary rates correlated with the evolution of body size, lifespan, or the first two principal components of body size and lifespan across *Myotis*, and found a number of genes enriched in pathways associated with innate immunity, gamete production, and various metabolic processes, consistent with our other results (**Figure S3D-E; Table S4**).

The longest-lived bat in our study, *M. lucifugus*, had an overrepresentation of pathways specifically associated with DNA double-strand break (DSB) repair when looking at both lineage-wide and node-specific enrichments in positive selection using the Reactome database[110] (**Figure 3C; Table S3**). This includes 35 out of 65 genes in the high-fidelity Homologous Recombination Repair pathway, and 21/37 members of the Homology-Directed Repair via Single Strand Annealing (**Figure 3C; Table S3**). These results suggest that *M. lucifugus* might have an enhanced response to DNA DSBs relative to other bats. To test this hypothesis, we assessed the tolerance of *M. lucifugus* to neocarzinostatin, a potent radiomimetic agent that induces DNA

double-strand breaks (**Figure 3D**), compared to *M. evotis*, three non-*Myotis* bats (*Eidolon helvum, Pteropus rodrigensis,* and *Rousettus lanosus*), and humans. At low doses of neocarzinostatin, *M. lucifugus* was the only species tested showing sensitivity to neocarzinostatin after 24 hours, with a drop in viability and concomitant increase in apoptosis. At high doses, *M. lucifugus* had the highest level of apoptosis and the greatest drop in viability of all the bats tested, although all bats were more resistant to DNA damage than humans. This is consistent with other long-lived species, including elephants[44,45,93], naked mole rats[52], and bowhead whales[48,111], where longevity and RICR are associated with an increased ability to clear out damaged cells. Together, these results support the hypothesis that *M. lucifugus* has evolved an enhanced DNA double-strand break response as predicted by genes exhibiting signatures of positive selection in this species.

Adaptation to DNA viruses

Amongst genes under selection, a substantial portion were involved with immunity, including members of the immunoglobulin and Cluster of Differentiation gene families. These genes exhibited some of the highest evolutionary rates (ω) in our dataset, suggesting that they are under strong selection in *Myotis* (**Table S3; Table S4**). Because immune pathways are only one aspect of host viral adaptation[112], we tested for adaptive signatures in virus-interacting proteins (VIPs) in *Myotis* and other bats. VIPs are host proteins that physically interact with viral proteins (e.g. *CD45*, **Figure 4A**), and can be proviral (contributing to viral infection, e.g. viral receptors), antiviral (protective against viral infection, e.g. interferons), or both depending on infection stage and virus type. Previous studies investigating positive selection across mammals have found an enrichment for adaptation among a set of 5,528 manually curated VIPs, defined as host proteins that have at least one experimentally verified physical interaction with a viral protein, RNA, or DNA[112].

By calculating an enrichment score from the ratio of positive selection in VIPs compared to their matched control genes using BUSTED-MH[113], we found that, like other mammals, *Myotis* show an enrichment for adaptation at VIPs (**Figure 4B; Table S5**). Physical host-virus interactions may not always result in fitness effects in the host. We therefore repeated our analysis using a gene set restricted to VIPs with experimental evidence of specific pro- or anti-viral effects, and thus with a stronger expectation of fitness effects. We observed an even stronger significant elevation in the ratio of positive selection in these proviral and antiviral VIPs (**Figure 4C; Table S5**), but no elevation in this ratio in other VIPs (**Figure 4D; Table S5**). This is consistent with the expectation of viral interaction as the cause of enrichment of positive selection in VIPs in bats[114]. We repeated this analysis using a dataset of 47 publicly-available non-*Myotis* bat genomes, and confirmed these same patterns across bats more broadly, even when excluding *Myotis* genomes (**Figure 4B** inset).

Previous work has suggested that bats may have different physiological responses to DNA and RNA viruses[115]. To determine if this was reflected in genomic VIP adaptation, we compared the enrichment of positive selection in VIPs that interact only with DNA viruses (DNA VIPs) to those that interact only with RNA viruses (RNA VIPs). Remarkably, we found that VIP adaptation in *Myotis* and other bats is driven by selection in DNA VIPs (**Figure 4E** and inset). This is in marked contrast to the observed pattern in RNA VIPs, which show no evidence of enrichment in adaptation (**Figure 4F** and inset). Note that this difference between DNA and RNA VIPs cannot be explained by a difference in the conservation of VIP status between the two. The vast majority of VIPs were discovered between human proteins and viruses that infect humans [114], and a concern could then be that those proteins that are RNA VIPs in humans have evolved faster than DNA VIPs in bats, ultimately resulting in the more frequent loss of their VIP status in bats. We can however exclude this possibility, since DNA and RNA VIPs have very similar average dN/dS ratios (Myotis, 0.2 vs. 0.18 respectively; non-Myotis bats, 0.163 vs. 0.153 respectively).

In contrast to what we observe in bats, VIP adaptation in humans is driven by positive selection in RNA - and not DNA - VIPs[112,116]. To investigate if DNA VIP-driven adaptation in bats is exceptional among mammals, we replicated these analyses across four other large mammalian orders that are well represented among publicly-available mammalian genomes: *Primates*, *Glires*, *Eeungulata*, and *Carnivora*. We found that while other mammalian orders show a mix of adaptation enrichments in both RNA and DNA VIPs, none show an absence of genome-wide enrichment of adaptation in RNA VIPs as observed in bats (**Figure S4**). These results highlight that bats, including *Myotis*, may have faced greater selective pressures from DNA viruses than from RNA viruses, in contrast to other mammals.

Evolution of structural variation within constrained karyotypes

With only six known exceptions, all *Myotis* species with cytological data have a conserved karyotype (60+ *Myotis spp.*: 2n = 44[117–121]; *M. annectans*: 2n = 46[119]; *M. laniger*: 2n = 48[120]; *M. bechsteinii*: 2n = 42[122]; *M. daubentoni*: 2n = 42[123]; *M. davidii*: 2n = 46 [124]; *M. macrodactylus*: 2n = 44/45[125,126]). This conserved *Myotis* karyotype, shared among species spread across six continents[1,2], consists of three large and one small metacentric autosomes; 17 small telocentric autosomes; and metacentric X and Y chromosomes [57,127]. Consistent with this broad cytological conservation, we find large scale synteny across the Nearctic *Myotis* in this study. However, structural variants (SVs) including inversions, duplications, and translocations are relatively common within chromosomes, especially in putative centromeric regions (**Figure 5A, B**).

We used SyRI[128] to identify SVs across pairwise alignments of Nearctic *Myotis* genomes relative to the outgroup *M. myotis* and identified 6,813 - 8,013 SVs per genome. Most of these events were small, with 97 - 99% of events under 10Kb. In the three large autosomes, which constitute ~30% of each genome, we cataloged an average of 509 SVs (**Table S6**). In contrast, in the small autosomes, constituting ~65% of each genome, we observed an average of 316 events, highlighting the distinct structural evolution between these chromosome types (**Table S6**). However, large (≥10Kb) duplications, large inverted duplications, and large inverted translocations were more common on small autosomes compared to the large autosomes (**Table S6**).

We also quantified the distribution of transposable elements (TEs) across chromosomes. Surprisingly, LINE elements were significantly enriched around the centromeres of all chromosomes, both metacentric and telocentric (**Figure 5B**); while this is rare in mammals, it has been described as a feature of Phyllostomid genomes[129]. In many cases, particularly in the 3 large metacentric chromosomes, LINE elements appear to have displaced other TEs. Rolling circle and SINE elements were particularly depleted concomitant with LINE enrichment. In contrast, SINE elements were enriched at telomeres. The concentration of segmental duplications is significantly correlated with TE density in each species (linear regression, $p < 0.01$; **Figure 5B; Figure S5J**) highlighting the possible importance of TEs in facilitating structural evolution.

One particularly striking example of structural evolution we identified is a ~20-Mb block at the subtelomeric end of chromosome V15 undergoing frequent and recurrent inversions and translocations in nearctic *Myotis* (**Figure 5A**). This region spans several immune-related genes including multiple members of interleukin signaling pathways, including IL-1 and IL-36. A 10Mb portion of this block was recently identified as a potential target of recent selection by adaptive introgression[69]. We identified between 2-3 major (8+ kb) blocks in this region exhibiting inversions between Nearctic *Myotis*, which correspond to similarly sized regions in the outgroup *M. myotis* (**Figure 5A; Table S5**). Additionally, we noted a depletion of DNA transposable elements at the boundaries of each inversion (**Figure 5B**), particularly for rolling circle (RC) and SINE elements. Both of

these elements can catalyze large-scale structural rearrangements via DNA damage repair and homologous recombination, respectively[130–134].

Gene duplications and losses can be drivers of evolution via dosage modification[135,136], sub- and neofunctionalization[137,138], regulatory network remodeling[139], and other processes[135]. We quantified gene gains and losses across *Myotis* relative to their single-copy human orthologs. Using CAFE[140], we found 38 gene families underwent significant expansions or contractions in at least one nearctic *Myotis* species (**Figure 5C**). However, gain and loss rates varied substantially across branches of the *Myotis* phylogeny. The terminal *M. auriculus* and *M. velifer* branches had ~4-fold more significant gene family expansions (37 and 35 families, respectively; **Figure 5C**) than other *Myotis* branches. In contrast, the terminal *M. californicus* and *M. yumanensis* branches had ~2-fold more significant contractions (24 and 23 families, respectively; **Figure 5C**) than other *Myotis* branches. We observe significant overrepresentation of pathways at FDR<=10% in only 4 gene sets: gene families that underwent significant expansions in *M. auriculus, M. velifer,* and *M. volans*; and genes that underwent significant contractions in *M. lucifugus* (**Figure S5A-H**). Many of these pathways were shared between all sets, including pathways involved in translation regulation; ROBO receptors and neuronal development; selenoprotein and selenocystine metabolism; and influenza life cycle (**Figure S5A-H**).

Given that many of the genes in these pathways are VIPs, we used the method of Huang et al (2023)[50] to test if VIP genes in particular underwent significant copy number changes relative to non-VIP genes. We found that while the birth-death rate of VIP genes is similar to that of other genes ($p = 0.071$), together VIP genes are significantly more likely to have undergone expansions and/or contractions on at least one branch of the *Myotis* family ($p < 0.001$; **Figure S5I-J**). This suggests that there is variation in gene family birth rates across species, but that VIPs are more dynamic across the Nearctic *Myotis* as a whole than other types of genes.

To further explore the functional impact of gene duplications we ranked genes by their maximum copy number across all genomes. We found that the gene families with the highest copy numbers were concentrated in pathways associated with cancer, aging, immunity, and olfaction (**Figure 5D**). One striking case is *FBXO31*, with ~2.4x more copies on average than the next most duplicated gene in *Myotis* (20-48 copies). FBXO31 is a SCF (SKP1-cullin-F-box) protein ligase involved in cell cycle regulation and DNA damage response, consisting of two functional domains: a F-Box domain and a CDK binding domain[141], and has previously been speculated as a driver of longevity in *Myotis*[96]. Quantifying *FBXO31* copy number across over 500 mammals using reciprocal best-hit BLAT, we found that this gene was more highly duplicated in *Myotis* than in any other mammal genome (**Figure 5E)**. Furthermore, while there were additional partial matches of non-canonical copies of *FBXO31* in non-*Myotis* species, all copies identified in *Myotis* are full-length genes with functional domains. To model the evolution of gene copy number, we used GeneRax[142] to reconcile the gene tree and species tree. GeneRax infers a gene family tree under scenarios of gene duplication and loss, taking into account the species tree. We found support for an original 14 duplications in the common ancestor of Nearctic *Myotis*, with subsequent gains and losses in each lineage (**Figure 5F**). These results highlight a massively expanded gene family in *Myotis* with potential consequences for the regulation of stress response and other processes.

An actively segregating, trans-species copy number polymorphism of the antiviral factor *PKR*

Our highly contiguous genome assemblies provide a unique opportunity to understand the evolutionary and functional dynamics of structural variation in adaptation. To illustrate this, we explored the antiviral innate immune Protein Kinase R (*PKR*/*EIF2AK2*), an interferon-stimulated gene with adaptive duplications unique to

Myotis[28]. Among our Neartic *Myotis* genome assemblies we resolved the structure of the two known structural haplotypes: H1, containing a single copy of *PKR* (*PKR2*); and H2, containing two tandemly duplicated copies of *PKR* (*PKR1* and *PKR2*; **Figure 6A**). Unexpectedly, we also identified a third haplotype - H3 - with three tandem duplicates of *PKR* (*PKR1*, *PKR2*, and a third copy). While 7 out of 9 *Myotis* species carried duplicated haplotypes (H2 in 6 species, H3 in *M. californicus*), to our surprise, 5 of these cases were heterozygous for the duplicated haplotype: (i.e. H1/H2 or H1/H3; **Figure 6B**). To determine the evolutionary history of these duplicates, we used GeneRax[142] to construct a tree from alignments of all *PKR* gene copies across Neartic *Myotis*, using *Pipistrellus pygmaeus* as a non-*Myotis* outgroup (**Figure 6C**). Our results suggest that *PKR2* is the canonical copy of *PKR*, and that *PKR1* originated from a single duplication event at the root of *Myotis*. Intriguingly, we observed that in the heterozygous species, both *PKR1* and *PKR2* on the duplicated haplotype clustered with other duplicated haplotypes, resulting in species tree violations for the canonical copy, *PKR2* (**Figure 6C**). These results highlight that both the duplicated and unduplicated haplotypes have likely been segregating for over 30 million years, representing an ancient trans-species polymorphism.

Protein Kinase R is a stress response and innate immune factor that interacts with viral or inverted Alu repeats dsRNAs via its dsRNA binding motifs (dsRBMs), leading to PKR auto-phosphorylation and dimerization[143,144]. Upon activation, PKR can then phosphorylate various molecules leading to protein translation shutdown and restriction of viral replication[143,144]. While the independent functional impacts of PKR1 and PKR2 were previously investigated[28], the effects of co-expressing both copies remains unknown. This is important because their final effects may be additive, synergistic or dominant negative, providing clues into why the PKR duplication is polymorphic both within and between *Myotis* species.

To better understand the functional consequences of possessing one or two copies of PKR, we investigated the effect of paralog co-expression on steady state protein levels, cell viability, protein translation shutdown and antiviral restriction (**Figure 6D-G**). We used PKR-KO Hela cells transfected with either *Myotis myotis* or *Myotis velifer* PKR1, PKR2, and PKR1+2. We found that the coexpression of *Myotis* Flag-PKR1 and Flag-PKR2 did not affect their protein expression levels (**Figure 6D; Figure S6**). Furthermore, coexpression of PKR1 and PKR2 led to a simple additive effect in their translation shutdown activity (**Figure 6E**), suggesting that neither copy is dominant negative. Using non-toxic doses of *Myotis* PKRs in the context of VSV-GFP (Vesicular stomatitis virus encoding a GFP reporter[145]) infections, we found that, although PKR1 and PKR2 are both antiviral[28], the coexpression of PKR1 and PKR2 is not beneficial against VSV (**Figure 6F**). Finally, because duplicated haplotypes may lead to increased doses of PKR in *Myotis* cells, we tested PKR impact on cell viability. We found that at low doses none of the *Myotis* PKRs affected cell viability. However, higher doses of PKRs led to more cell toxicity, potentially resulting in a tradeoff (**Figure 6G**). Altogether, this may explain why PKR is rarely duplicated in mammals, and why both single- and duplicate haplotypes of the loci are segregating across several *Myotis* species. These genomic and functional results highlight the impact of an unfixed gene duplicate which may play a role in adaptation to viral infections.

Discussion

A functionally empowered approach to comparative genomics

Bats are widely known for their long lifespan, cancer resistance, and viral tolerance[6,10,11,36,73,92,146–148]. As highly complex and pleiotropic processes, the genes and mechanisms underlying these phenotypes can be challenging to identify. Comparative approaches to identify the genetic bases of these traits are constrained by

the availability of high-quality genomes, annotations, and functional resources for validation. These challenges are exacerbated in the case of rapidly-evolving phenotypes, such as host-pathogen interactions.

Here we outline an approach that enables functional comparative biology by generating cell lines from wing punches of wild caught bats for genome assembly, comparative genomics, and functional follow up. Cell lines are generated from minimally-invasive biopsies collected in the field thus avoiding disturbing natural populations. Given the high density of bat species concentrated at single locations world-wide[149,150] it is feasible to collect wing punches from a large number of individuals across a wide phylogenetic range; these wing punches can be used to generate cell lines and sequencing libraries for reference genomes in a matter of weeks. This is an important advance, not only for efforts to expand genetic resources across the tree of life[151–153], but for conservation genomics. As our approach can generate genomic resources from minimal material gathered via non-lethal sampling, it is well-suited for the study of rare or endangered species for which acquiring sufficient amounts of material can be challenging.

Evolution of lifespan and cancer risk in a new phylogenetic context

The evolution of body size and lifespan across mammals - and the rapid evolution of lifespan in *Yinpterochiroptera* in particular - has major implications for the co-evolution of cancer risk and resistance. While models of body size evolution are well-studied in mammals[7,46,75,77] the evolution of lifespan is less well understood. By explicitly modeling the evolution of lifespan separately from body size, we recapitulate the extant relationship between body size and lifespan across mammals in evolutionary time. Contrary to prior work, we show that overall bats exhibit allometric lifespan scaling, comparable to other mammals. However, two bat clades - *Myotis* and *Phyllostomidae* - exhibit distinct trends with *Myotis* demonstrating an increased rate of change in lifespan given body size compared to other mammals. This altered scaling of longevity in *Myotis* has dramatic consequences for their intrinsic, per-cell cancer risk and for the evolution of tumor-suppressor genes and pathways. While cancer risk scales linearly with body size, it scales over time as a power law of 6[86,89,90]. Meanwhile, while mammalian body sizes span a 10^6 range of masses, they only span a 10^2 range of lifespans[16,154]. Unlike other systems where the evolution of cancer resistance has been driven by rapid changes in body size[44–46,51,94,97], the body size of *Myotis* has not significantly changed since their common ancestor. Instead, the rapid and repeated changes in lifespan across an order of magnitude in *Myotis* lead to some of the most significant changes in intrinsic cancer risk seen across mammals.

We found a number of genes under selection across multiple longevity-associated pathways, consistent with the pleiotropic nature of the aging process. These include members of canonical longevity pathways such as mTOR-IGF signaling, DNA damage repair, oxidative stress, and the senescence-associated secretory phenotype. We additionally identified selection in various pathways that have likely emerged as a result of the unique biology of bats, including genes at the intersection of immunity and senescence, such as Serapin-family genes; genes in metabolic pathways including amino acid metabolism; and pervasive selection observed in the ferroptosis pathway, which sits at the intersection of bats' extreme oxidative challenges, metabolic demands, immune function, and cancer resistance. By quantifying the relative contributions of genes under selection to cancer-related pathways at each node, we found significant enrichment of these processes across the phylogeny, especially at nodes undergoing the greatest changes in lifespan and cancer risk.

While the implications of an increased cancer risk are clear, the implications of decreases in relative cancer risk are less so. As expected by Peto's Paradox, we observe an overrepresentation of cancer-related pathways among genes under selection at nodes experiencing high increases in relative cancer risk, consistent with patterns observed in other vertebrates[46,48,51,53,76,94–97]. However, we also observed an enrichment in cancer-

related pathway representation among genes under selection in nodes with significant decreases in cancer risk (e.g: *M. thysanodes, M. velifer*). This combination of low intrinsic cancer risk alongside the persistence of cancer-related adaptations, has been observed previously in sloths and armadillos[76]. Intriguingly, these species demonstrate some of the lowest known rates of cancer among mammals. While no reports or studies of neoplasia rates have been published in *Myotis*, the use of *in vitro* models of carcinogenesis provides a promising avenue for comparative studies of cancer resistance under controlled conditions. In agreement with our results, *in vitro* and xenograft transplant models have shown that cells of long-lived bats, including *M. lucifugus,* are more resistant to carcinogenesis than shorter-lived bats and other mammals[148]. Such studies provide a reliable route for the experimental validation of the evolution of cancer resistance in species where *in vivo* work would otherwise prove ethically or practically intractable.

Viral adaptation and immunity

The nature of viral tolerance and infectious disease adaptation in bats has major implications for understanding their role as zoonotic reservoirs and mechanisms of infectious disease adaptation. Here we focus on Virus Interacting Proteins (VIPs) that influence viral response and contain vital information about the nature of host adaptation to viruses[112]. By integrating comparative analyses of VIP adaptation, VIP and immune gene family expansion and contraction, and functional experiments, we show that virus adaptation in bats is mostly driven by DNA viruses, as opposed to RNA viruses; we recapitulate and expand on previous results related to positive selection in immune genes and immune gene family expansion, contraction, and loss; and demonstrate complex patterns of structural variation, including a segregating duplication of protein kinase R (PKR), a major protein involved in the antiviral innate immune system, that has functional relevance in its activity against viruses.

The remarkable dominance of adaptation in response to DNA viruses in bats is in contrast with viral adaptation in humans and other primates, which is driven by RNA viruses[116,155]; and in other mammals, in which virus adaptation is driven by a combination of DNA and RNA viruses. Most zoonoses, including those hosted by bats, are RNA viruses[10], making this especially important in understanding the dynamics of emerging infectious diseases. This novel finding complements previous observations that bats are more likely than other mammals to asymptomatically harbor RNA viruses, while being more susceptible themselves to other pathogens, such as fungi[115]. This suggests multiple, non-exclusive, possibilities. First, bats may have some other form of response to RNA viruses that sufficiently reduces the fitness effect of these viruses such that the associated VIPs did not adapt as strongly. Second, our result does not imply that bats have not adapted to RNA viruses, rather that adaptation to RNA viruses does not exceed the genomic baseline adaptation, while adaptation to DNA viruses does. Indeed, bats are known to mount adaptive immune responses to some RNA viruses and the strength of their immune response can have complex interactions with hibernation and reproduction[10]. It has been previously suggested that bats may rely more strongly on adaptive immunity in response to RNA viruses than to other pathogens[115], though evolutionary functional analyses have also found evidence of innate immune adaptation to RNA viruses, including *RTP4* to flaviviruses[156] and *OAS1* to SARS-COVs[157]. This is consistent with our findings of positive selection and gene family expansion in adaptive immune proteins.

While previous work has shown associations between gene family size and certain phenotypic traits in bats[36,54,158,159], confirmation of functional effects of copy number is rare. By resolving individual haplotypes in these nine *Myotis* species, we were able to confirm a single duplication event at the origin of *Myotis PKR1* and *PKR2*. We further demonstrate functional implications of copy number variation in Protein kinase R, as previously shown in functional evolutionary studies (eg. Jacquet et al. 2022). These results are especially interesting in the light of other studies that have found trans-species polymorphisms related to immune genes[160]. This further

illustrates the importance of high-quality genome assemblies and annotations, to distinguish copy number variation between haplotypes, as well as between functional copies and pseudogenes[161].

The role of agonistic pleiotropy in driving adaptations in bats

Multiple hypotheses have been proposed to connect the unique physiology and ecology of bats with the evolution of remarkable adaptations such as viral infection tolerance, stress tolerance, and exceptional longevity[146]. Hypothesized drivers of disease resistance and longevity evolution in bats include the evolution of flight (e.g. “flight as fever” hypothesis[162], though this hypothesis has recently been critiqued[163], the disposable soma hypothesis[164]); metabolic state[165]; torpor[6]; and other adaptations to specific environments[9,159,166,167]. Additionally, many studies have highlighted the intersection of one or more of these traits, including a relationship between hibernation and both longevity[6] and disease resistance[115]. Our results are consistent with an *agonistic* pleiotropy hypothesis, wherein genetic adaptations for many specific traits (e.g. physiological stress to flight, hibernation, DNA virus innate immunity) may prove beneficial to other seemingly-unrelated traits (e.g. cancer resistance, cellular homeostasis, longevity).

Consistent with this, many of the genes and pathways highlighted in this study have been found to play vital roles across physiological traits in bats and other species. For example, two genes under selection in neartic *Myotis* - *FTH1* and *IGFN1* - have been implicated in functional studies as key hibernation genes[168–170], viral interacting proteins[171–174], and as pro-longevity genes[175–177]. Similarly, many DNA VIPs such as *BRCA1/2* and *POLG* represent core DNA maintenance genes essential for cancer resistance and longevity[52,178–184]; the existence of active DNA transposable elements such as *Helitron* in *Myotis* may provide another selective pressure on DNA repair genes[185]. Beyond individual genes, many of the overarching pathways under selection in *Myotis*, such as those associated with inflammation, senescence, and ferroptosis lie directly at the intersection of aging-related immune processes[36,54,56,78,170,175,186–191]. While these results suggest the possibility that traits such as cancer risk, cellular homeostasis, and antiviral response have evolved in tandem due to pleiotropic selection at overlapping points in bats’ evolutionary histories, further functional validation will be required to disentangle the functional impacts of these genetic changes and disambiguate the drivers of selection.

Acknowledgements

PacBio HiFi sequencing was done by the DNA Technologies and Expression Analysis Cores at the UC Davis Genome Center, supported by NIH Shared Instrumentation Grant 1S10OD010786-01. This material is based in part upon High Performance Computing (HPC) resources supported by the University of Arizona TRIF, UITS, and Research, Innovation, and Impact (RII) and maintained by the UArizona Research Technologies department. This research used the Savio computational cluster resource provided by the Berkeley Research Computing program at the University of California, Berkeley (supported by the UC Berkeley Chancellor, Vice Chancellor for Research, and Chief Information Officer). Computations were performed, in part, on the Vermont Advanced Computing Core. We thank the members of the LP2L team (CIRI) for helpful discussions.

MEL was funded by NSF PRFB #2010884, and a Dovetail Tree of Life Grant. JMV was funded by NSF PRFB #2109915 and NIH NIA T32AG000266. DE was funded by NIH NIGMS MIRA grant 5R35GM142677. PHS was funded by NIH NIGMS grant R35GM142916 and by the Vallee Scholars Award. LE was funded by a grant from the Agence Nationale de la Recherche (ANR, #ANR-202-CE15-0020-01 to LE) and by the CNRS. LE and DE were further funded by a grant from the Joint Call for Proposals between the CNRS and the University of Arizona

(International Research Center, IRC, 2021-2024). LE, DE, PHS and SP were further funded by the International Research Project (IRP) RAPIDvBAT from the CNRS, the University of Arizona and the University of California, Berkeley.

Image attributions for the bat photos featured in Figure 1: J. Scott Altenbach (*M. thysanodes, M. velifer*); Rick & Nora Bowers (*M. occultus*); U.S. National Park Service (*M. auriculus*); Frank Carey (*M. californicus*); Michael Durham (*M. evotis*); J. N. Stuart (*M. volans*); and SMBishop & the Wikimedia Foundation (*M. lucifugus*).

Author Contributions:

Conceptualization, J.M.V., M.E.L., D.E., P.H.S., L.E., D.F., M.B.; Methodology, J.M.V., M.E.L., D.E., P.H.S., L.E., G.G.S.; Software, J.M.V., M.E.L., D.E., P.H.S., L.E., T.M.L.; Validation, J.M.V., M.E.L., D.E., P.H.S., L.E., J.P.V.M.; Formal Analysis, J.M.V., M.E.L., D.E., P.H.S., L.E., S.M., A.L.C., D.M., S.V.; Investigation, J.M.V., M.E.L., S.M., M.B., D.F., G.G.S., L.G., Z.R.H., M.H., W.K., T.M.L., A.L.C., S.M., D.M., S.L., J.L., C.R., S.L.R.C., M.S., K.S., W.T., J.D.T., S.V., R.M., M.B., J.P.V.M., S.P., L.E., D.E., P.H.S.; Resources, J.M.V., M.E.L., D.E., P.H.S., L.E., M.B., D.F., G.G.S., L.G., Z.R.H., M.H., W.K., T.M.L., A.L.C., S.M., D.M., S.L., J.L., C.R., S.L.R.C., M.S., K.S., W.T., J.D.T., S.V., R.M., M.B.; Data Curation, J.M.V., M.E.L., S.M., M.B., D.F., G.G.S., L.G., Z.R.H., M.H., W.K., T.M.L., A.L.C., S.M., D.M., S.L., J.L., C.R., S.L.R.C., M.S., K.S., W.T., J.D.T., S.V., R.M., M.B., J.P.V.M., S.P., L.E., D.E., P.H.S.; Writing - Original Draft, J.M.V., M.E.L., D.E., P.H.S., L.E., S.M., J.L.; Writing - Review & Editing, J.M.V., M.E.L., S.M., M.B., D.F., G.G.S., L.G., Z.R.H., M.H., W.K., T.M.L., A.L.C., S.M., D.M., S.L., J.L., C.R., S.L.R.C., M.S., K.S., W.T., J.D.T., S.V., R.M., M.B., J.P.V.M., S.P., L.E., D.E., P.H.S.; Visualization, J.M.V., M.E.L., D.E., P.H.S., L.E., S.M., A.L.C.; Supervision, J.M.V., M.E.L., D.E., P.H.S., L.E.; Project Administration, J.M.V., M.E.L., D.E., P.H.S., L.E.; Funding Acquisition, J.M.V., M.E.L., D.E., P.H.S., L.E.

Declaration of Interests:

The authors declare no competing interests.

References

1. Wilson, D.E., and Reeder, D.M. (2005). Mammal Species of the World: A Taxonomic and Geographic Reference (JHU Press).

2. Simmons, N.B., and Cirranello, A.L. Bat Species of the World: A Taxonomic and Geographic Database. https://batnames.org/.

3. Teeling, E.C., Hedges, S.B., and Kumar, S. (2009). Bats (Chiroptera). The timetree of life, 499–503.

4. Rietbergen, T.B., Ostende, L.W. van den H., Aase, A., Jones, M.F., Medeiros, E.D., and Simmons, N.B. (2023). The Oldest Known Bat Skeletons and Their Implications for Eocene Chiropteran Diversification. PLoS One *18*, e0283505. https://doi.org/10.1371/journal.pone.0283505.

5. Kumar, S., Stecher, G., Suleski, M., and Hedges, S.B. (2017). TimeTree: A Resource for

Timelines, Timetrees, and Divergence Times. Mol. Biol. Evol. *34*, 1812–1819. https://doi.org/10.1093/molbev/msx116.

6. Wilkinson, G.S., and Adams, D.M. (2019). Recurrent Evolution of Extreme Longevity in Bats. Biol. Lett. *15*, 20180860. https://doi.org/10.1098/rsbl.2018.0860.

7. Moyers Arévalo, R.L., Amador, L.I., Almeida, F.C., and Giannini, N.P. (2020). Evolution of Body Mass in Bats: Insights from a Large Supermatrix Phylogeny. J. Mamm. Evol. *27*, 123–138. https://doi.org/10.1007/s10914-018-9447-8.

8. Datzmann, T., von Helversen, O., and Mayer, F. (2010). Evolution of Nectarivory in Phyllostomid Bats (Phyllostomidae Gray, 1825, Chiroptera: Mammalia). BMC Evol. Biol. *10*, 165. https://doi.org/10.1186/1471-2148-10-165.

9. Camacho, J., Bernal-Rivera, A., Peña, V., Morales-Sosa, P., Robb, S., Russell, J., Yi, K., Wang, Y., Tsuchiya, D., Murillo-García, O.E., et al. (2023). Sugar assimilation underlying dietary evolution of Neotropical bats. bioRxiv, 2023.07.02.547432. https://doi.org/10.1101/2023.07.02.547432.

10. Hayman, D.T.S., Bowen, R.A., Cryan, P.M., McCracken, G.F., O'Shea, T.J., Peel, A.J., Gilbert, A., Webb, C.T., and Wood, J.L.N. (2013). Ecology of zoonotic infectious diseases in bats: current knowledge and future directions. Zoonoses Public Health *60*, 2–21. https://doi.org/10.1111/zph.12000.

11. Irving, A.T., Ahn, M., Goh, G., Anderson, D.E., and Wang, L.-F. (2021). Lessons from the host defences of bats, a unique viral reservoir. Nature *589*, 363–370. https://doi.org/10.1038/s41586-020-03128-0.

12. Morales, A.E., Ruedi, M., Field, K., and Carstens, B.C. (2019). Diversification rates have no effect on the convergent evolution of foraging strategies in the most speciose genus of bats, Myotis. Evolution *73*, 2263–2280. https://doi.org/10.1111/evo.13849.

13. Gunnell, G.F., Smith, R., and Smith, T. (2017). 33 million year old Myotis (Chiroptera, Vespertilionidae) and the rapid global radiation of modern bats. PLoS One *12*, e0172621. https://doi.org/10.1371/journal.pone.0172621.

14. Ruedi, M., Stadelmann, B., Gager, Y., Douzery, E.J.P., Francis, C.M., Lin, L.-K., Guillén-Servent, A., and Cibois, A. (2013). Molecular Phylogenetic Reconstructions Identify East Asia as the Cradle for the Evolution of the Cosmopolitan Genus Myotis (Mammalia, Chiroptera). Mol. Phylogenet. Evol. *69*, 437–449. https://doi.org/10.1016/j.ympev.2013.08.011.

15. Tacutu, R., Craig, T., Budovsky, A., Wuttke, D., Lehmann, G., Taranukha, D., Costa, J., Fraifeld, V.E., and de Magalhães, J.P. (2013). Human Ageing Genomic Resources: Integrated Databases and Tools for the Biology and Genetics of Ageing. Nucleic Acids Res. *41*, D1027–D1033. https://doi.org/10.1093/nar/gks1155.

16. Jones, K.E., Bielby, J., Cardillo, M., Fritz, S.A., O'Dell, J., Orme, C.D.L., Safi, K., Sechrest, W., Boakes, E.H., Carbone, C., et al. (2009). PanTHERIA: A Species-Level Database of Life History, Ecology, and Geography of Extant and Recently Extinct Mammals. Ecology *90*, 2648–2648. https://doi.org/10.1890/08-1494.1.

17. Austad, S.N. (2010). Methusaleh's Zoo: How Nature Provides Us with Clues for Extending Human Health Span. J. Comp. Pathol. *142*, S10–S21. https://doi.org/10.1016/j.jcpa.2009.10.024.

18. Austad, S.N., and Fischer, K.E. (1991). Mammalian Aging, Metabolism, and Ecology: Evidence

from the Bats and Marsupials. J. Gerontol. *46*, B47–B53. https://doi.org/10.1093/geronj/46.2.b47.

19. Podlutsky, A.J., Khritankov, A.M., Ovodov, N.D., and Austad, S.N. (2005). A new field record for bat longevity. J. Gerontol. A Biol. Sci. Med. Sci. *60*, 1366–1368. https://doi.org/10.1093/gerona/60.11.1366.

20. Wilson, D.E., and Tyson, E.L. (1970). Longevity Records for Artibeus Jamaicensis and Myotis Nigricans. J. Mammal. *51*, 203. https://doi.org/10.2307/1378570.

21. Stadelmann, B., Lin, L.-K., Kunz, T.H., and Ruedi, M. (2007). Molecular Phylogeny of New World \emphMyotis (Chiroptera, Vespertilionidae) Inferred from Mitochondrial and Nuclear DNA Genes. Mol. Phylogenet. Evol. *43*, 32–48. https://doi.org/10.1016/j.ympev.2006.06.019.

22. Agnarsson, I., Zambrana-Torrelio, C.M., Flores-Saldana, N.P., and May-Collado, L.J. (2011). A time-calibrated species-level phylogeny of bats (Chiroptera, Mammalia). PLoS Curr. *3*, RRN1212. https://doi.org/10.1371/currents.RRN1212.

23. Seltmann, A., Troxell, S.A., Schad, J., Fritze, M., Bailey, L.D., Voigt, C.C., and Czirják, G.Á. (2022). Author Correction: Differences in acute phase response to bacterial, fungal and viral antigens in greater mouse-eared bats (Myotis myotis). Sci. Rep. *12*, 21144. https://doi.org/10.1038/s41598-022-25685-2.

24. Armero, A., Li, R., Bienes, K.M., Chen, X., Li, J., Xu, S., Chen, Y., Hughes, A.C., Berthet, N., and Wong, G. (2022). Myotis fimbriatus virome, a window to virus diversity and evolution in the genus Myotis. Viruses *14*, 1899. https://doi.org/10.3390/v14091899.

25. He, X., Korytář, T., Zhu, Y., Pikula, J., Bandouchova, H., Zukal, J., and Köllner, B. (2014). Establishment of Myotis Myotis Cell Lines - Model for Investigation of Host-Pathogen Interaction in a Natural Host for Emerging Viruses. PLoS One *9*, e109795. https://doi.org/10.1371/journal.pone.0109795.

26. Hayward, J.A., Tachedjian, M., Johnson, A., Irving, A.T., Gordon, T.B., Cui, J., Nicolas, A., Smith, I., Boyd, V., Marsh, G.A., et al. (2022). Unique Evolution of Antiviral Tetherin in Bats. J. Virol. *96*, e0115222. https://doi.org/10.1128/jvi.01152-22.

27. Fernandes, A.P., Águeda-Pinto, A., Pinheiro, A., Rebelo, H., and Esteves, P.J. (2022). Evolution of TRIM5 and TRIM22 in Bats Reveals a Complex Duplication Process. Viruses *14*. https://doi.org/10.3390/v14020345.

28. Jacquet, S., Culbertson, M., Zhang, C., El Filali, A., De La Myre Mory, C., Pons, J.-B., Filippi-Codaccioni, O., Lauterbur, M.E., Ngoubangoye, B., Duhayer, J., et al. (2022). Adaptive duplication and genetic diversification of protein kinase R contribute to the specificity of bat-virus interactions. Sci Adv *8*, eadd7540. https://doi.org/10.1126/sciadv.add7540.

29. Jacquet, S., Pontier, D., and Etienne, L. (2020). Rapid Evolution of HERC6 and Duplication of a Chimeric HERC5/6 Gene in Rodents and Bats Suggest an Overlooked Role of HERCs in Mammalian Immunity. Front. Immunol. *11*, 605270. https://doi.org/10.3389/fimmu.2020.605270.

30. Chomel, B., Stuckey, M., Boulouis, H., and Aguilar Setién, Á. (2014). Bat-Related Zoonoses. Zoonoses - Infections Affecting Humans and Animals, 697–714. https://doi.org/10.1007/978-94-017-9457-2_28.

31. Guth, S., Mollentze, N., Renault, K., Streicker, D.G., Visher, E., Boots, M., and Brook, C.E. (2022). Bats host the most virulent-but not the most dangerous-zoonotic viruses. Proc. Natl. Acad. Sci. U.

S. A. *119*, e2113628119. https://doi.org/10.1073/pnas.2113628119.

32. Williams, E.P., Spruill-Harrell, B.M., Taylor, M.K., Lee, J., Nywening, A.V., Yang, Z., Nichols, J.H., Camp, J.V., Owen, R.D., and Jonsson, C.B. (2021). Common themes in zoonotic spillover and disease emergence: Lessons learned from bat- and rodent-borne RNA viruses. Viruses *13*, 1509. https://doi.org/10.3390/v13081509.

33. Mollentze, N., and Streicker, D.G. (2020). Viral zoonotic risk is homogenous among taxonomic orders of mammalian and avian reservoir hosts. Proc. Natl. Acad. Sci. U. S. A. *117*, 9423–9430. https://doi.org/10.1073/pnas.1919176117.

34. Tenthorey, J.L., Emerman, M., and Malik, H.S. (2022). Evolutionary Landscapes of Host-Virus Arms Races. Annu. Rev. Immunol. *40*, 271–294. https://doi.org/10.1146/annurev-immunol-072621-084422.

35. Klunk, J., Vilgalys, T.P., Demeure, C.E., Cheng, X., Shiratori, M., Madej, J., Beau, R., Elli, D., Patino, M.I., Redfern, R., et al. (2022). Evolution of immune genes is associated with the Black Death. Nature *611*, 312–319. https://doi.org/10.1038/s41586-022-05349-x.

36. Jebb, D., Huang, Z., Pippel, M., Hughes, G.M., Lavrichenko, K., Devanna, P., Winkler, S., Jermiin, L.S., Skirmuntt, E.C., Katzourakis, A., et al. (2020). Six reference-quality genomes reveal evolution of bat adaptations. Nature *583*, 578–584. https://doi.org/10.1038/s41586-020-2486-3.

37. Mynard, P., Algar, A.C., Lancaster, L.T., Bocedi, G., Fahri, F., Gubry-Rangin, C., Lupiyaningdyah, P., Nangoy, M., Osborne, O.G., Papadopulos, A.S.T., et al. (2023). Impact of phylogenetic tree completeness and mis-specification of sampling fractions on trait dependent diversification models. Syst. Biol. *72*, 106–119. https://doi.org/10.1093/sysbio/syad001.

38. Garamszegi, L.Z., and Møller, A.P. (2010). Effects of sample size and intraspecific variation in phylogenetic comparative studies: a meta-analytic review. Biol. Rev. Camb. Philos. Soc. *85*, 797–805. https://doi.org/10.1111/j.1469-185X.2010.00126.x.

39. Garamszegi, L.Z. ed. (2014). Modern Phylogenetic Comparative Methods and Their Application in Evolutionary Biology: Concepts and Practice (Springer) https://doi.org/10.1007/978-3-662-43550-2.

40. Nabhan, A.R., and Sarkar, I.N. (2012). The impact of taxon sampling on phylogenetic inference: a review of two decades of controversy. Brief. Bioinform. *13*, 122–134. https://doi.org/10.1093/bib/bbr014.

41. Li, S., Vazquez, J.M., and Sudmant, P.H. (2023). The Evolution of Aging and Lifespan. Trends Genet. *0*. https://doi.org/10.1016/j.tig.2023.08.005.

42. López-Otín, C., Blasco, M.A., Partridge, L., Serrano, M., and Kroemer, G. (2013). The Hallmarks of Aging. Cell *153*, 1194–1217. https://doi.org/10.1016/j.cell.2013.05.039.

43. Kolora, S.R.R., Owens, G.L., Vazquez, J.M., Stubbs, A., Chatla, K., Jainese, C., Seeto, K., McCrea, M., Sandel, M.W., Vianna, J.A., et al. (2021). Origins and Evolution of Extreme Life Span in Pacific Ocean Rockfishes. Science *374*, 842–847. https://doi.org/10.1126/science.abg5332.

44. Sulak, M., Fong, L., Mika, K., Chigurupati, S., Yon, L., Mongan, N.P., Emes, R.D., and Lynch, V.J. (2016). Correction: TP53 copy number expansion is associated with the evolution of increased body size and an enhanced DNA damage response in elephants. Elife *5*. https://doi.org/10.7554/eLife.24307.

45. Vazquez, J.M., Sulak, M., Chigurupati, S., and Lynch, V.J. (2018). A Zombie LIF Gene in Elephants Is Upregulated by TP53 to Induce Apoptosis in Response to DNA Damage. Cell Rep. *24*, 1765–1776. https://doi.org/10.1016/j.celrep.2018.07.042.

46. Vazquez, J.M., and Lynch, V.J. (2021). Pervasive Duplication of Tumor Suppressors in Afrotherians during the Evolution of Large Bodies and Reduced Cancer Risk. Elife *10*, e65041. https://doi.org/10.7554/eLife.65041.

47. Davies, K.T.J., Tsagkogeorga, G., Bennett, N.C., Dávalos, L.M., Faulkes, C.G., and Rossiter, S.J. (2014). Molecular Evolution of Growth Hormone and Insulin-like Growth Factor 1 Receptors in Long-Lived, Small-Bodied Mammals. Gene *549*, 228–236. https://doi.org/10.1016/j.gene.2014.07.061.

48. Vazquez, J.M., Kraft, M., and Lynch, V.J. (2022). A CDKN2C retroduplication in Bowhead whales is associated with the evolution of extremely long lifespans and alerted cell cycle dynamics. bioRxiv, 2022.09.07.506958. https://doi.org/10.1101/2022.09.07.506958.

49. Foote, A.D., Liu, Y., Thomas, G.W.C., Vinař, T., Alföldi, J., Deng, J., Dugan, S., van Elk, C.E., Hunter, M.E., Joshi, V., et al. (2015). Convergent evolution of the genomes of marine mammals. Nat. Genet. *47*, 272–275. https://doi.org/10.1038/ng.3198.

50. Huang, Z., Jiang, C., Gu, J., Uvizl, M., Power, S., Douglas, D., and Kacprzyk, J. (2023). Duplications of Human Longevity-Associated Genes Across Placental Mammals. Genome Biol. Evol. *15*. https://doi.org/10.1093/gbe/evad186.

51. Glaberman, S., Bulls, S.E., Vazquez, J.M., Chiari, Y., and Lynch, V.J. (2021). Concurrent Evolution of Antiaging Gene Duplications and Cellular Phenotypes in Long-Lived Turtles. Genome Biol. Evol. *13*, evab244. https://doi.org/10.1093/gbe/evab244.

52. MacRae, S.L., Croken, M.M., Calder, R.B., Aliper, A., Milholland, B., White, R.R., Zhavoronkov, A., Gladyshev, V.N., Seluanov, A., Gorbunova, V., et al. (2015). DNA Repair in Species with Extreme Lifespan Differences. Aging *7*, 1171–1184. https://doi.org/10.18632/aging.100866.

53. Baines, C., Meitern, R., Kreitsberg, R., and Sepp, T. (2022). Comparative study of the evolution of cancer gene duplications across fish. Evol. Appl. *15*, 1834–1845. https://doi.org/10.1111/eva.13481.

54. Moreno Santillán, D.D., Lama, T.M., Gutierrez Guerrero, Y.T., Brown, A.M., Donat, P., Zhao, H., Rossiter, S.J., Yohe, L.R., Potter, J.H., Teeling, E.C., et al. (2021). Large-scale genome sampling reveals unique immunity and metabolic adaptations in bats. Mol. Ecol. *30*, 6449–6467. https://doi.org/10.1111/mec.16027.

55. Scheben, A., Mendivil Ramos, O., Kramer, M., Goodwin, S., Oppenheim, S., Becker, D.J., Schatz, M.C., Simmons, N.B., Siepel, A., and McCombie, W.R. (2023). Long-Read Sequencing Reveals Rapid Evolution of Immunity- and Cancer-Related Genes in Bats. Genome Biol. Evol. *15*. https://doi.org/10.1093/gbe/evad148.

56. Tian, S., Zeng, J., Jiao, H., Zhang, D., Zhang, L., Lei, C.-Q., Rossiter, S.J., and Zhao, H. (2023). Comparative analyses of bat genomes identify distinct evolution of immunity in Old World fruit bats. Sci Adv *9*, eadd0141. https://doi.org/10.1126/sciadv.add0141.

57. Sotero-Caio, C.G., Baker, R.J., and Volleth, M. (2017). Chromosomal evolution in Chiroptera. Genes (Basel) *8*. https://doi.org/10.3390/genes8100272.

58. Nachtweide, S., and Stanke, M. (2019). Multi-Genome Annotation with AUGUSTUS. Methods Mol. Biol. *1962*, 139–160. https://doi.org/10.1007/978-1-4939-9173-0_8.

59. Lomsadze, A., Ter-Hovhannisyan, V., Chernoff, Y.O., and Borodovsky, M. (2005). Gene identification in novel eukaryotic genomes by self-training algorithm. Nucleic Acids Res. *33*, 6494–6506. https://doi.org/10.1093/nar/gki937.

60. Shumate, A., and Salzberg, S.L. (2021). Liftoff: accurate mapping of gene annotations. Bioinformatics.

61. Kirilenko, B.M., Munegowda, C., Osipova, E., Jebb, D., Sharma, V., Blumer, M., Morales, A.E., Ahmed, A.-W., Kontopoulos, D.-G., Hilgers, L., et al. (2023). Integrating gene annotation with orthology inference at scale. Science *380*, eabn3107. https://doi.org/10.1126/science.abn3107.

62. Li, H. (2023). Protein-to-genome alignment with miniprot. Bioinformatics.

63. Simão, F.A., Waterhouse, R.M., Ioannidis, P., Kriventseva, E.V., and Zdobnov, E.M. (2015). BUSCO: assessing genome assembly and annotation completeness with single-copy orthologs. Bioinformatics *31*, 3210–3212. https://doi.org/10.1093/bioinformatics/btv351.

64. Manni, M., Berkeley, M.R., Seppey, M., and Zdobnov, E.M. (2021). BUSCO: assessing genomic data quality and beyond. Current Protocols *1*.

65. Curti, J., Fraser, D., Escalona, M., Fairbairn, C.W., Sacco, S., Sahasrabudhe, R., Nguyen, O., Seligmann, W., Sudmant, P.H., Toffelmier, E., et al. (2023). A Genome Assembly of the Yuma Myotis Bat, Myotis Yumanensis. J. Hered., esad053. https://doi.org/10.1093/jhered/esad053.

66. Amador, L.I., Moyers Arévalo, R.L., Almeida, F.C., Catalano, S.A., and Giannini, N.P. (2018). Bat Systematics in the Light of Unconstrained Analyses of a Comprehensive Molecular Supermatrix. J. Mamm. Evol. *25*, 37–70. https://doi.org/10.1007/s10914-016-9363-8.

67. Upham, N.S., Esselstyn, J.A., and Jetz, W. (2019). Inferring the mammal tree: Species-level sets of phylogenies for questions in ecology, evolution, and conservation. PLoS Biol. *17*, e3000494. https://doi.org/10.1371/journal.pbio.3000494.

68. Korstian, J.M., Paulat, N.S., Platt, R.N., Stevens, R.D., and Ray, D.A. (2022). SINE-Based Phylogenomics Reveal Extensive Introgression and Incomplete Lineage Sorting in Myotis. Genes *13*, 399. https://doi.org/10.3390/genes13030399.

69. Foley, N.M., Harris, A.J., Bredemeyer, K.R., Ruedi, M., Puechmaille, S.J., Teeling, E.C., Criscitiello, M.F., and Murphy, W.J. (2024). Karyotypic stasis and swarming influenced the evolution of viral tolerance in a species-rich bat radiation. Cell Genom *4*, 100482. https://doi.org/10.1016/j.xgen.2023.100482.

70. UniProt Consortium (2023). UniProt: The universal protein knowledgebase in 2023. Nucleic Acids Res. *51*, D523–D531. https://doi.org/10.1093/nar/gkac1052.

71. dos Reis, M., and Yang, Z. (2011). Approximate likelihood calculation on a phylogeny for Bayesian estimation of divergence times. Mol. Biol. Evol. *28*, 2161–2172. https://doi.org/10.1093/molbev/msr045.

72. Yang, Z. (2007). PAML 4: phylogenetic analysis by maximum likelihood. Mol. Biol. Evol. *24*, 1586–1591. https://doi.org/10.1093/molbev/msm088.

73. Brunet-Rossinni, A.K., and Austad, S.N. (2004). Ageing studies on bats: a review. Biogerontology *5*, 211–222. https://doi.org/10.1023/B:BGEN.0000038022.65024.d8.

74. Wilkinson, G.S., and South, J.M. (2002). Life History, Ecology and Longevity in Bats. Aging Cell *1*, 124–131. https://doi.org/10.1046/j.1474-9728.2002.00020.x.

75. Puttick, M.N., and Thomas, G.H. (2015). Fossils and living taxa agree on patterns of body mass evolution: a case study with Afrotheria. Proc. Biol. Sci. *282*, 20152023. https://doi.org/10.1098/rspb.2015.2023.

76. Vazquez, J.M., Pena, M.T., Muhammad, B., Kraft, M., Adams, L.B., and Lynch, V.J. (2022). Parallel Evolution of Reduced Cancer Risk and Tumor Suppressor Duplications in Xenarthra. Elife *11*, e82558. https://doi.org/10.7554/eLife.82558.

77. Slater, G.J., Goldbogen, J.A., and Pyenson, N.D. (2017). Independent evolution of baleen whale gigantism linked to Plio-Pleistocene ocean dynamics. Proc. Biol. Sci. *284*. https://doi.org/10.1098/rspb.2017.0546.

78. Ricklefs, R.E. (2010). Life-history connections to rates of aging in terrestrial vertebrates. Proc. Natl. Acad. Sci. U. S. A. *107*, 10314–10319. https://doi.org/10.1073/pnas.1005862107.

79. Tillquist, R.C., Shoemaker, L.G., Knight, K.B., and Clauset, A. (2016). The evolution of primate body size: Left-skewness, maximum size, and Cope's Rule. bioRxiv, 092866. https://doi.org/10.1101/092866.

80. Kuparinen, A., Yeung, E., and Hutchings, J.A. (2023). Correlation between body size and longevity: New analysis and data covering six taxonomic classes of vertebrates. Acta Oecol. (Montrouge) *119*, 103917. https://doi.org/10.1016/j.actao.2023.103917.

81. Montgomery, S.H., Geisler, J.H., McGowen, M.R., Fox, C., Marino, L., and Gatesy, J. (2013). The evolutionary history of cetacean brain and body size: Cetacean brain evolution. Evolution *67*, 3339–3353. https://doi.org/10.1111/evo.12197.

82. Pyenson, N.D., and Sponberg, S.N. (2011). Reconstructing body size in extinct crown Cetacea (neoceti) using allometry, phylogenetic methods and tests from the fossil record. J. Mamm. Evol. *18*, 269–288. https://doi.org/10.1007/s10914-011-9170-1.

83. Delsuc, F., Gibb, G.C., Kuch, M., Billet, G., Hautier, L., Southon, J., Rouillard, J.-M., Fernicola, J.C., Vizcaíno, S.F., MacPhee, R.D.E., et al. (2016). The phylogenetic affinities of the extinct glyptodonts. Curr. Biol. *26*, R155–R156. https://doi.org/10.1016/j.cub.2016.01.039.

84. Argot, C. (2008). Changing Views in Paleontology: The Story of a Giant (Megatherium, Xenarthra). In Mammalian Evolutionary Morphology Vertebrate Paleobiology and Paleoanthropology Series., E. J. Sargis and M. Dagosto, eds. (Springer Netherlands), pp. 37–50. https://doi.org/10.1007/978-1-4020-6997-0_3.

85. Raj Pant, S., Goswami, A., and Finarelli, J.A. (2014). Complex body size trends in the evolution of sloths (Xenarthra: Pilosa). BMC Evol. Biol. *14*, 184. https://doi.org/10.1186/s12862-014-0184-1.

86. Armitage, P. (1985). Multistage Models of Carcinogenesis. Environ. Health Perspect. *63*, 195–201. https://doi.org/10.1289/ehp.8563195.

87. Armitage, P., and Doll, R. (2004). The Age Distribution of Cancer and a Multi-Stage Theory of Carcinogenesis. Br. J. Cancer *91*, 6602297. https://doi.org/10.1038/sj.bjc.6602297.

88. Peto, R., Roe, F.J., Lee, P.N., Levy, L., and Clack, J. (1975). Cancer and ageing in mice and men. Br. J. Cancer *32*, 411–426. https://doi.org/10.1038/bjc.1975.242.

89. Peto, R. (2015). Quantitative Implications of the Approximate Irrelevance of Mammalian Body Size and Lifespan to Lifelong Cancer Risk. Philos. Trans. R. Soc. Lond. B Biol. Sci. *370*, 20150198. https://doi.org/10.1098/rstb.2015.0198.

90. Nunney, L. (2018). Size Matters: Height, Cell Number and a Person's Risk of Cancer. Proc. R. Soc. B *285*, 20181743. https://doi.org/10.1098/rspb.2018.1743.

91. Caulin, A.F., and Maley, C.C. (2011). Peto's Paradox: evolution's prescription for cancer prevention. Trends Ecol. Evol. *26*, 175–182. https://doi.org/10.1016/j.tree.2011.01.002.

92. Vincze, O., Colchero, F., Lemaître, J.-F., Conde, D.A., Pavard, S., Bieuville, M., Urrutia, A.O., Ujvari, B., Boddy, A.M., Maley, C.C., et al. (2022). Cancer risk across mammals. Nature *601*, 263–267. https://doi.org/10.1038/s41586-021-04224-5.

93. Abegglen, L.M., Caulin, A.F., Chan, A., Lee, K., Robinson, R., Campbell, M.S., Kiso, W.K., Schmitt, D.L., Waddell, P.J., Bhaskara, S., et al. (2015). Potential Mechanisms for Cancer Resistance in Elephants and Comparative Cellular Response to DNA Damage in Humans. JAMA *314*, 1850–1860. https://doi.org/10.1001/jama.2015.13134.

94. Tollis, M., Robbins, J., Webb, A., Kuderna, L.F.K., Caulin, A.F., Garcia, J.D., Bérubé, M., Pourmand, N., Marquès-Bonet, T., O'Connell, M., et al. (2019). Return to the sea, get huge, beat cancer: An analysis of cetacean genomes including an assembly for the humpback whale (Megaptera novaeangliae). Mol. Biol. Evol. *36*, 1746–1763. https://doi.org/10.1093/molbev/msz099.

95. Tollis, M., Schneider-Utaka, A.K., and Maley, C.C. (2020). The evolution of human cancer gene duplications across mammals. Mol. Biol. Evol. *37*, 2875–2886. https://doi.org/10.1093/molbev/msaa125.

96. Caulin, A.F., Graham, T.A., Wang, L.-S., and Maley, C.C. (2015). Solutions to Peto's paradox revealed by mathematical modelling and cross-species cancer gene analysis. Philos. Trans. R. Soc. Lond. B Biol. Sci. *370*, 20140222. https://doi.org/10.1098/rstb.2014.0222.

97. Nair, N.U., Cheng, K., Naddaf, L., Sharon, E., Pal, L.R., Rajagopal, P.S., Unterman, I., Aldape, K., Hannenhalli, S., Day, C.-P., et al. (2022). Cross-species identification of cancer resistance-associated genes that may mediate human cancer risk. Sci. Adv. *8*, eabj7176. https://doi.org/10.1126/sciadv.abj7176.

98. Smith, M.D., Wertheim, J.O., Weaver, S., Murrell, B., Scheffler, K., and Kosakovsky Pond, S.L. (2015). Less is more: an adaptive branch-site random effects model for efficient detection of episodic diversifying selection. Mol. Biol. Evol. *32*, 1342–1353. https://doi.org/10.1093/molbev/msv022.

99. Hanahan, D., and Weinberg, R.A. (2011). Hallmarks of Cancer: The Next Generation. Cell *144*, 646–674. https://doi.org/10.1016/j.cell.2011.02.013.

100. Hanahan, D., and Weinberg, R.A. (2000). The Hallmarks of Cancer. Cell *100*, 57–70. https://doi.org/10.1016/S0092-8674(00)81683-9.

101. Hanahan, D. (2022). Hallmarks of Cancer: New Dimensions. Cancer Discov. *12*, 31–46. https://doi.org/10.1158/2159-8290.CD-21-1059.

102. Wertheim, J.O., Murrell, B., Smith, M.D., Kosakovsky Pond, S.L., and Scheffler, K. (2015). RELAX: detecting relaxed selection in a phylogenetic framework. Mol. Biol. Evol. *32*, 820–832. https://doi.org/10.1093/molbev/msu400.

103. Wang, A., Zhu, F., Liang, R., Li, D., and Li, B. (2019). Regulation of T cell differentiation and function by ubiquitin-specific proteases. Cell. Immunol. *340*, 103922. https://doi.org/10.1016/j.cellimm.2019.103922.

104. Meng, Y., Hong, C., Yang, S., Qin, Z., Yang, L., and Huang, Y. (2023). Roles of USP9X in cellular functions and tumorigenesis (Review). Oncol. Lett. *26*, 506. https://doi.org/10.3892/ol.2023.14093.

105. Dohmen, M., Krieg, S., Agalaridis, G., Zhu, X., Shehata, S.N., Pfeiffenberger, E., Amelang, J., Bütepage, M., Buerova, E., Pfaff, C.M., et al. (2020). AMPK-dependent activation of the Cyclin Y/CDK16 complex controls autophagy. Nat. Commun. *11*, 1032. https://doi.org/10.1038/s41467-020-14812-0.

106. Wang, X., Liu, R., Li, S., Xia, W., Guo, H., Yao, W., Liang, X., Lu, Y., and Zhang, H. (2023). The roles, molecular interactions, and therapeutic value of CDK16 in human cancers. Biomed. Pharmacother. *164*, 114929. https://doi.org/10.1016/j.biopha.2023.114929.

107. Katoh, Y., and Katoh, M. (2009). FGFR2-related pathogenesis and FGFR2-targeted therapeutics (Review). Int. J. Mol. Med. *23*, 307–311. https://doi.org/10.3892/ijmm_00000132.

108. Wang, K., Lai, C., Li, T., Wang, C., Wang, W., Ni, B., Bai, C., Zhang, S., Han, L., Gu, H., et al. (2018). Basic fibroblast growth factor protects against influenza A virus-induced acute lung injury by recruiting neutrophils. J. Mol. Cell Biol. *10*, 573–585. https://doi.org/10.1093/jmcb/mjx047.

109. Kowalczyk, A., Meyer, W.K., Partha, R., Mao, W., Clark, N.L., and Chikina, M. (2019). RERconverge: an R package for associating evolutionary rates with convergent traits. Bioinformatics *35*, 4815–4817. https://doi.org/10.1093/bioinformatics/btz468.

110. Milacic, M., Beavers, D., Conley, P., Gong, C., Gillespie, M., Griss, J., Haw, R., Jassal, B., Matthews, L., May, B., et al. (2024). The reactome pathway knowledgebase 2024. Nucleic Acids Res. *52*, D672–D678. https://doi.org/10.1093/nar/gkad1025.

111. Firsanov, D., Zacher, M., Tian, X., Zhao, Y., George, J.C., Sformo, T.L., Tombline, G., Biashad, S.A., Gilman, A., Hamilton, N., et al. (2023). DNA repair and anti-cancer mechanisms in the longest-living mammal: the bowhead whale. bioRxiv, 2023.05.07.539748. https://doi.org/10.1101/2023.05.07.539748.

112. Enard, D., Cai, L., Gwennap, C., and Petrov, D.A. (2016). Viruses are a dominant driver of protein adaptation in mammals. Elife *5*. https://doi.org/10.7554/eLife.12469.

113. Murrell, B., Weaver, S., Smith, M.D., Wertheim, J.O., Murrell, S., Aylward, A., Eren, K., Pollner, T., Martin, D.P., Smith, D.M., et al. (2015). Gene-wide identification of episodic selection. Mol. Biol. Evol. *32*, 1365–1371. https://doi.org/10.1093/molbev/msv035.

114. Souilmi, Y., Lauterbur, M.E., Tobler, R., Huber, C.D., Johar, A.S., Moradi, S.V., Johnston, W.A., Krogan, N.J., Alexandrov, K., and Enard, D. (2021). An ancient viral epidemic involving host coronavirus interacting genes more than 20,000 years ago in East Asia. Curr. Biol. *31*, 3704. https://doi.org/10.1016/j.cub.2021.07.052.

115. Brook, C.E., and Dobson, A.P. (2015). Bats as “special” reservoirs for emerging zoonotic pathogens. Trends Microbiol. *23*, 172–180. https://doi.org/10.1016/j.tim.2014.12.004.

116. Enard, D., and Petrov, D.A. (2018). Evidence that RNA Viruses Drove Adaptive Introgression between Neanderthals and Modern Humans. Cell *175*, 360–371.e13. https://doi.org/10.1016/j.cell.2018.08.034.

117. Volleth, M. (2012). Variations on a theme: Karyotype comparison in Eurasian Myotis species and implications for phylogeny. Vespertilio *16*, 329–350.

118. McBee, K. (1986). Standard karyology of nine species of vespertilionid bats (Chiroptera: Vespertilionidae) from Thailand. Annals of Carnegie Museum *55*, 95–116.

119. Bickham, J.W., McBee, K., and Schlitter, D.A. (1986). Chromosomal variation among seven species of Myotis (Chiroptera: Vespertilionidae). J. Mammal. *67*, 746–750. https://doi.org/10.2307/1381139.

120. Zhang, W.D. (1984). A study on karyotype of Myotis chinensis and M. laniger Peter. J Anhui Normal Univ *7*, 42–47.

121. Zima, J. (1985). Synopsis of karyotypes of vespertilionid bats (Mammalia: Chiroptera). Acta Univ. Carol. Biol *1981*, 311–329.

122. Karataş, A., Sözen, M., Özkurt, Ş., and Matur, F. (2007). Karyology of three bat species of the genusMyotis (M. myotis, M. bechsteinii, M. brandtii)(Chiroptera: Vespertilionidae) from Turkey. Zool. Middle East *40*, 5–9. https://doi.org/10.1080/09397140.2007.10638198.

123. Bovey, R. (1949). Chromosones of Chiroptera and Insectivora.

124. Yi, W.U., and Harada, M. (2006). Karyology of seven species of bats (Mammalia: Chiroptera) from Guangdong, China. Shou Lei Xue Bao *26*, 403.

125. Yoshitaka Obara, Takafumi Tomiyasu, and Kazuo Saitoh (1976). CHROMOSOME STUDIES IN THE JAPANESE VESPERTILIONID BATS: I. KARYOTYPIC VARIATIONS IN MYOTIS MACRODACTYLUS TEMMINCK. Jpn. J. Genet. *51*, 201–206.

126. Vujošević, M., Rajičić, M., and Blagojević, J. (2018). B Chromosomes in Populations of Mammals Revisited. Genes *9*. https://doi.org/10.3390/genes9100487.

127. O'Brien, S.J., Menninger, J.C., and Nash, W.G. (2006). Atlas of Mammalian Chromosomes (John Wiley & Sons).

128. Goel, M., Sun, H., Jiao, W.-B., and Schneeberger, K. (2019). SyRI: finding genomic rearrangements and local sequence differences from whole-genome assemblies. Genome Biol. *20*, 277. https://doi.org/10.1186/s13059-019-1911-0.

129. de Sotero-Caio, C.G., Cabral-de-Mello, D.C., Calixto, M. da S., Valente, G.T., Martins, C., Loreto, V., de Souza, M.J., and Santos, N. (2017). Centromeric enrichment of LINE-1 retrotransposons and its significance for the chromosome evolution of Phyllostomid bats. Chromosome Res. *25*, 313–325. https://doi.org/10.1007/s10577-017-9565-9.

130. Kosek, D., Grabundzija, I., Lei, H., Bilic, I., Wang, H., Jin, Y., Peaslee, G.F., Hickman, A.B., and Dyda, F. (2021). The large bat Helitron DNA transposase forms a compact monomeric assembly that buries and protects its covalently bound 5'-transposon end. Mol. Cell *81*, 4271–4286.e4. https://doi.org/10.1016/j.molcel.2021.07.028.

131. Ducani, C., Bernardinelli, G., and Högberg, B. (2014). Rolling circle replication requires single-

stranded DNA binding protein to avoid termination and production of double-stranded DNA. Nucleic Acids Res. *42*, 10596–10604. https://doi.org/10.1093/nar/gku737.

132. Thomas, J., Phillips, C.D., Baker, R.J., and Pritham, E.J. (2014). Rolling-circle transposons catalyze genomic innovation in a mammalian lineage. Genome Biol. Evol. *6*, 2595–2610. https://doi.org/10.1093/gbe/evu204.

133. Balachandran, P., Walawalkar, I.A., Flores, J.I., Dayton, J.N., Audano, P.A., and Beck, C.R. (2022). Transposable element-mediated rearrangements are prevalent in human genomes. Nat. Commun. *13*, 7115. https://doi.org/10.1038/s41467-022-34810-8.

134. Ait Saada, A., Guo, W., Costa, A.B., Yang, J., Wang, J., and Lobachev, K.S. (2023). Widely spaced and divergent inverted repeats become a potent source of chromosomal rearrangements in long single-stranded DNA regions. Nucleic Acids Res. *51*, 3722–3734. https://doi.org/10.1093/nar/gkad153.

135. Kondrashov, F.A. (2011). Gene Dosage and Duplication. In Evolution after Gene Duplication, K. Dittmar and D. Liberles, eds. (John Wiley & Sons), pp. 57–76.

136. Kondrashov, F.A., Rogozin, I.B., Wolf, Y.I., and Koonin, E.V. (2002). Selection in the evolution of gene duplications. Genome Biol. *3*, RESEARCH0008. https://doi.org/10.1186/gb-2002-3-2-research0008.

137. Rastogi, S., and Liberles, D.A. (2005). Subfunctionalization of duplicated genes as a transition state to neofunctionalization. BMC Evol. Biol. *5*, 28. https://doi.org/10.1186/1471-2148-5-28.

138. Assis, R., and Bachtrog, D. (2013). Neofunctionalization of young duplicate genes in Drosophila. Proc. Natl. Acad. Sci. U. S. A. *110*, 17409–17414. https://doi.org/10.1073/pnas.1313759110.

139. Tirosh, I., and Barkai, N. (2007). Comparative analysis indicates regulatory neofunctionalization of yeast duplicates. Genome Biol. *8*, R50. https://doi.org/10.1186/gb-2007-8-4-r50.

140. Mendes, F.K., Vanderpool, D., Fulton, B., and Hahn, M.W. (2021). CAFE 5 models variation in evolutionary rates among gene families. Bioinformatics *36*, 5516–5518. https://doi.org/10.1093/bioinformatics/btaa1022.

141. Duan, S., Moro, L., Qu, R., Simoneschi, D., Cho, H., Jiang, S., Zhao, H., Chang, Q., de Stanchina, E., Arbini, A.A., et al. (2021). Loss of FBXO31-mediated degradation of DUSP6 dysregulates ERK and PI3K-AKT signaling and promotes prostate tumorigenesis. Cell Rep. *37*, 109870. https://doi.org/10.1016/j.celrep.2021.109870.

142. Morel, B., Kozlov, A.M., Stamatakis, A., and Szöllősi, G.J. (2020). GeneRax: A Tool for Species-Tree-Aware Maximum Likelihood-Based Gene Family Tree Inference under Gene Duplication, Transfer, and Loss. Mol. Biol. Evol. *37*, 2763–2774. https://doi.org/10.1093/molbev/msaa141.

143. Kaufman, R.J. (1999). Double-stranded RNA-activated protein kinase mediates virus-induced apoptosis: a new role for an old actor. Proc. Natl. Acad. Sci. U. S. A. *96*, 11693–11695. https://doi.org/10.1073/pnas.96.21.11693.

144. García, M.A., Gil, J., Ventoso, I., Guerra, S., Domingo, E., Rivas, C., and Esteban, M. (2006). Impact of protein kinase PKR in cell biology: from antiviral to antiproliferative action. Microbiol. Mol. Biol. Rev. *70*, 1032–1060. https://doi.org/10.1128/MMBR.00027-06.

145. Ostertag, D., Hoblitzell-Ostertag, T.M., and Perrault, J. (2007). Overproduction of double-stranded

RNA in vesicular stomatitis virus-infected cells activates a constitutive cell-type-specific antiviral response. J. Virol. *81*, 503–513. https://doi.org/10.1128/JVI.01218-06.

146. Lagunas-Rangel, F.A. (2020). Why do bats live so long?—Possible molecular mechanisms. Biogerontology *21*, 1–11. https://doi.org/10.1007/s10522-019-09840-3.

147. Chionh, Y.T., Cui, J., Koh, J., Mendenhall, I.H., Ng, J.H.J., Low, D., Itahana, K., Irving, A.T., and Wang, L.-F. (2019). High basal heat-shock protein expression in bats confers resistance to cellular heat/oxidative stress. Cell Stress Chaperones *24*, 835–849. https://doi.org/10.1007/s12192-019-01013-y.

148. Hua, R., Ma, Y.-S., Yang, L., Hao, J.-J., Hua, Q.-Y., Shi, L.-Y., Yao, X.-Q., Zhi, H.-Y., and Liu, Z. (2024). Experimental evidence for cancer resistance in a bat species. Nat. Commun. *15*, 1401. https://doi.org/10.1038/s41467-024-45767-1.

149. Peixoto, F.P., Braga, P.H.P., and Mendes, P. (2018). A synthesis of ecological and evolutionary determinants of bat diversity across spatial scales. BMC Ecol. *18*, 18. https://doi.org/10.1186/s12898-018-0174-z.

150. USGS (2022). North American Bat Ranges. http://dds.cr.usgs.gov/pub/data/nationalatlas/bat000p010g_nt00373.tar.gz http://dds.cr.usgs.gov/pub/data/nationalatlas/bat000p010g_nt00373.tar.gz.

151. Rhie, A., McCarthy, S.A., Fedrigo, O., Damas, J., Formenti, G., Koren, S., Uliano-Silva, M., Chow, W., Fungtammasan, A., Kim, J., et al. (2021). Towards complete and error-free genome assemblies of all vertebrate species. Nature *592*, 737–746. https://doi.org/10.1038/s41586-021-03451-0.

152. The Darwin Tree of Life Project Consortium (2022). Sequence Locally, Think Globally: The Darwin Tree of Life Project. Proceedings of the National Academy of Sciences *119*, e2115642118. https://doi.org/10.1073/pnas.2115642118.

153. Lewin, H.A., Richards, S., Lieberman Aiden, E., Allende, M.L., Archibald, J.M., Bálint, M., Barker, K.B., Baumgartner, B., Belov, K., Bertorelle, G., et al. (2022). The Earth BioGenome Project 2020: Starting the Clock. Proceedings of the National Academy of Sciences *119*, e2115635118. https://doi.org/10.1073/pnas.2115635118.

154. Tacutu, R., Thornton, D., Johnson, E., Budovsky, A., Barardo, D., Craig, T., Diana, E., Lehmann, G., Toren, D., Wang, J., et al. (2018). Human Ageing Genomic Resources: new and updated databases. Nucleic Acids Res. *46*, D1083–D1090. https://doi.org/10.1093/nar/gkx1042.

155. Enard, D., and Petrov, D.A. (2020). Ancient RNA virus epidemics through the lens of recent adaptation in human genomes. Philos. Trans. R. Soc. Lond. B Biol. Sci. *375*, 20190575. https://doi.org/10.1098/rstb.2019.0575.

156. Boys, I.N., Xu, E., Mar, K.B., De La Cruz-Rivera, P.C., Eitson, J.L., Moon, B., and Schoggins, J.W. (2020). RTP4 is a potent IFN-inducible anti-flavivirus effector engaged in a host-virus arms race in bats and other mammals. Cell Host Microbe *28*, 712–723.e9. https://doi.org/10.1016/j.chom.2020.09.014.

157. Lytras, S., Wickenhagen, A., Sugrue, E., Stewart, D.G., Swingler, S., Sims, A., Jackson Ireland, H., Davies, E.L., Ludlam, E.M., Li, Z., et al. (2023). Resurrection of 2'-5'-oligoadenylate synthetase 1 (OAS1) from the ancestor of modern horseshoe bats blocks SARS-CoV-2 replication. PLoS Biol. *21*, e3002398. https://doi.org/10.1371/journal.pbio.3002398.

158. Tsagkogeorga, G., Müller, S., Dessimoz, C., and Rossiter, S.J. (2017). Comparative genomics reveals contraction in olfactory receptor genes in bats. Sci. Rep. *7*, 259. https://doi.org/10.1038/s41598-017-00132-9.

159. Gutiérrez-Guerrero, Y.T., Ibarra-Laclette, E., Martínez Del Río, C., Barrera-Redondo, J., Rebollar, E.A., Ortega, J., León-Paniagua, L., Urrutia, A., Aguirre-Planter, E., and Eguiarte, L.E. (2020). Genomic consequences of dietary diversification and parallel evolution due to nectarivory in leaf-nosed bats. Gigascience *9*. https://doi.org/10.1093/gigascience/giaa059.

160. Xie, S.S., Huang, C.H., Reid, M.E., Blancher, A., and Blumenfeld, O.O. (1997). The glycophorin A gene family in gorillas: structure, expression, and comparison with the human and chimpanzee homologues. Biochem. Genet. *35*, 59–76. https://doi.org/10.1023/a:1022212630370.

161. Gustavsson, E.K., Sethi, S., Gao, Y., Brenton, J.W., García-Ruiz, S., Zhang, D., Garza, R., Reynolds, R.H., Evans, J.R., Chen, Z., et al. (2024). The annotation of GBA1 has been concealed by its protein-coding pseudogene GBAP1. Sci. Adv. *10*, eadk1296. https://doi.org/10.1126/sciadv.adk1296.

162. O'Shea, T.J., Cryan, P.M., Cunningham, A.A., Fooks, A.R., Hayman, D.T.S., Luis, A.D., Peel, A.J., Plowright, R.K., and Wood, J.L.N. (2014). Bat flight and zoonotic viruses. Emerg. Infect. Dis. *20*, 741–745. https://doi.org/10.3201/eid2005.130539.

163. Levesque, D.L., Boyles, J.G., Downs, C.J., and Breit, A.M. (2021). High Body Temperature is an Unlikely Cause of High Viral Tolerance in Bats. J. Wildl. Dis. *57*, 238–241. https://doi.org/10.7589/JWD-D-20-00079.

164. Kirkwood, T.B.L. (2017). The disposable soma theory. The evolution of senescence in the tree of life, 23–39.

165. Toshkova, N., Zhelyzkova, V., Reyes-Ruiz, A., Haerens, E., de Castro Deus, M., Lacombe, R.V., Lecerf, M., Gonzalez, G., Jouvenet, N., Planchais, C., et al. (2024). Temperature sensitivity of bat antibodies links metabolic state of bats with antigen-recognition diversity. Nat. Commun. *15*, 5878. https://doi.org/10.1038/s41467-024-50316-x.

166. Mandl, J.N., Schneider, C., Schneider, D.S., and Baker, M.L. (2018). Going to bat(s) for studies of disease tolerance. Front. Immunol. *9*, 2112. https://doi.org/10.3389/fimmu.2018.02112.

167. Pei, G., Balkema-Buschmann, A., and Dorhoi, A. (2024). Disease tolerance as immune defense strategy in bats: One size fits all? PLoS Pathog. *20*, e1012471. https://doi.org/10.1371/journal.ppat.1012471.

168. Vermillion, K.L., Anderson, K.J., Hampton, M., and Andrews, M.T. (2015). Gene expression changes controlling distinct adaptations in the heart and skeletal muscle of a hibernating mammal. Physiol. Genomics *47*, 58–74. https://doi.org/10.1152/physiolgenomics.00108.2014.

169. Lam, B., Kajderowicz, K.M., Keys, H.R., Roessler, J.M., Frenkel, E.M., Kirkland, A., Bisht, P., El-Brolosy, M.A., Jaenisch, R., Bell, G.W., et al. (2024). Multi-species genome-wide CRISPR screens identify GPX4 as a conserved suppressor of cold-induced cell death. bioRxivorg, 2024.07.25.605098. https://doi.org/10.1101/2024.07.25.605098.

170. Sone, M., and Yamaguchi, Y. (2024). Cold resistance of mammalian hibernators ~ a matter of ferroptosis? Front. Physiol. *15*, 1377986. https://doi.org/10.3389/fphys.2024.1377986.

171. Kaelber, J.T., Demogines, A., Harbison, C.E., Allison, A.B., Goodman, L.B., Ortega, A.N., Sawyer,

S.L., and Parrish, C.R. (2012). Evolutionary reconstructions of the transferrin receptor of Caniforms supports canine parvovirus being a re-emerged and not a novel pathogen in dogs. PLoS Pathog. *8*, e1002666. https://doi.org/10.1371/journal.ppat.1002666.

172. Demogines, A., Abraham, J., Choe, H., Farzan, M., and Sawyer, S.L. (2013). Dual host-virus arms races shape an essential housekeeping protein. PLoS Biol. *11*, e1001571. https://doi.org/10.1371/journal.pbio.1001571.

173. Kerr, S.A., Jackson, E.L., Lungu, O.I., Meyer, A.G., Demogines, A., Ellington, A.D., Georgiou, G., Wilke, C.O., and Sawyer, S.L. (2015). Computational and functional analysis of the virus-receptor interface reveals host range trade-offs in New World arenaviruses. J. Virol. *89*, 11643–11653. https://doi.org/10.1128/JVI.01408-15.

174. Kaur, H., Kalayjian, R., Wu, K., Tassiopoulos, K., Palella, F., Taiwo, B., Bush, W., Hileman, C., Bedimo, R., Koletar, S., et al. (2022). Associations of L-Ferritin and Tim-1 with frailty measures in people with HIV: a cross-sectional and longitudinal study. Lancet Healthy Longev. *3*, S5. https://doi.org/10.1016/s2666-7568(22)00066-6.

175. Kim, J., Jo, Y., Cho, D., and Ryu, D. (2022). L-threonine promotes healthspan by expediting ferritin-dependent ferroptosis inhibition in C. elegans. Nat. Commun. *13*, 6554. https://doi.org/10.1038/s41467-022-34265-x.

176. Daghlas, I., and Gill, D. (2021). Genetically predicted iron status and life expectancy. Clin. Nutr. *40*, 2456–2459. https://doi.org/10.1016/j.clnu.2020.06.025.

177. Perez, K., Ciotlos, S., McGirr, J., Limbad, C., Doi, R., Nederveen, J.P., Nilsson, M.I., Winer, D.A., Evans, W., Tarnopolsky, M., et al. (2022). Single nuclei profiling identifies cell specific markers of skeletal muscle aging, frailty, and senescence. Aging (Albany NY) *14*, 9393–9422. https://doi.org/10.18632/aging.204435.

178. Trifunovic, A., Wredenberg, A., Falkenberg, M., Spelbrink, J.N., Rovio, A.T., Bruder, C.E., Bohlooly-Y, M., Gidlöf, S., Oldfors, A., Wibom, R., et al. (2004). Premature ageing in mice expressing defective mitochondrial DNA polymerase. Nature *429*, 417–423. https://doi.org/10.1038/nature02517.

179. Van Goethem, G., Dermaut, B., Löfgren, A., Martin, J.J., and Van Broeckhoven, C. (2001). Mutation of POLG is associated with progressive external ophthalmoplegia characterized by mtDNA deletions. Nat. Genet. *28*, 211–212. https://doi.org/10.1038/90034.

180. Cao, L., Li, W., Kim, S., Brodie, S.G., and Deng, C.-X. (2003). Senescence, aging, and malignant transformation mediated by p53 in mice lacking the Brca1 full-length isoform. Genes Dev. *17*, 201–213. https://doi.org/10.1101/gad.1050003.

181. Vijg, J., Perls, T., Franceschi, C., and van Orsouw, N.J. (2001). BRCA1 gene sequence variation in centenarians. Ann. N. Y. Acad. Sci. *928*, 85–96. https://doi.org/10.1111/j.1749-6632.2001.tb05639.x.

182. Fearon, E.R. (1997). Human cancer syndromes: clues to the origin and nature of cancer. Science *278*, 1043–1050. https://doi.org/10.1126/science.278.5340.1043.

183. Donoho, G., Brenneman, M.A., Cui, T.X., Donoviel, D., Vogel, H., Goodwin, E.H., Chen, D.J., and Hasty, P. (2003). Deletion of Brca2 exon 27 causes hypersensitivity to DNA crosslinks, chromosomal instability, and reduced life span in mice. Genes Chromosomes Cancer *36*, 317–331. https://doi.org/10.1002/gcc.10148.

184. Wooster, R., Bignell, G., Lancaster, J., Swift, S., Seal, S., Mangion, J., Collins, N., Gregory, S., Gumbs, C., and Micklem, G. (1995). Identification of the breast cancer susceptibility gene BRCA2. Nature *378*, 789–792. https://doi.org/10.1038/378789a0.

185. Ray, D.A., Feschotte, C., Pagan, H.J.T., Smith, J.D., Pritham, E.J., Arensburger, P., Atkinson, P.W., and Craig, N.L. (2008). Multiple Waves of Recent DNA Transposon Activity in the Bat, Myotis Lucifugus. Genome Res. *18*, 717–728. https://doi.org/10.1101/gr.071886.107.

186. Sotgia, S., Zinellu, A., Mangoni, A.A., Serra, R., Pintus, G., Caruso, C., Deiana, L., and Carru, C. (2017). Cellular immune activation in Sardinian middle-aged, older adults and centenarians. Exp. Gerontol. *99*, 133–137. https://doi.org/10.1016/j.exger.2017.10.005.

187. Lee, K.-A., Flores, R.R., Jang, I.H., Saathoff, A., and Robbins, P.D. (2022). Immune senescence, immunosenescence and aging. Front. Aging *3*, 900028. https://doi.org/10.3389/fragi.2022.900028.

188. Yousefzadeh, M.J., Flores, R.R., Zhu, Y., Schmiechen, Z.C., Brooks, R.W., Trussoni, C.E., Cui, Y., Angelini, L., Lee, K.-A., McGowan, S.J., et al. (2021). An aged immune system drives senescence and ageing of solid organs. Nature *594*, 100–105. https://doi.org/10.1038/s41586-021-03547-7.

189. Lee, C.-S., Chang, C.-H., Chen, C.-Y., Shih, C.-Y., Peng, J.-K., Huang, H.-L., Chen, P.-Y., Huang, T.-L., Chen, C.-Y., and Tsai, J.-S. (2022). Upregulation of cluster of differentiation 36 mRNA expression in peripheral blood mononuclear cells correlates with frailty severity in older adults. J. Cachexia Sarcopenia Muscle *13*, 1948–1955. https://doi.org/10.1002/jcsm.13003.

190. Kimmel, J.C., Yi, N., Roy, M., Hendrickson, D.G., and Kelley, D.R. (2021). Differentiation reveals latent features of aging and an energy barrier in murine myogenesis. Cell Rep. *35*, 109046. https://doi.org/10.1016/j.celrep.2021.109046.

191. Tian, Y., Lu, J., Hao, X., Li, H., Zhang, G., Liu, X., Li, X., Zhao, C., Kuang, W., Chen, D., et al. (2020). FTH1 inhibits ferroptosis through ferritinophagy in the 6-OHDA model of Parkinson's disease. Neurotherapeutics *17*, 1796–1812. https://doi.org/10.1007/s13311-020-00929-z.

192. Jonathan Sleeman, Center Director, USGS National Wildlife Health Center (2020). NWHC Operations During the COVID-19 Pandemic and Information About Coronaviruses in Wildlife.

193. White-Nose Syndrome Disease Management Working Group National White-Nose Syndrome Decontamination Protocol.

194. Dudchenko, O., Batra, S.S., Omer, A.D., Nyquist, S.K., Hoeger, M., Durand, N.C., Shamim, M.S., Machol, I., Lander, E.S., Aiden, A.P., et al. (2017). De novo assembly of the Aedes aegypti genome using Hi-C yields chromosome-length scaffolds. Science *356*, 92–95. https://doi.org/10.1126/science.aal3327.

195. Lindblad-Toh, K., Garber, M., Zuk, O., Lin, M.F., Parker, B.J., Washietl, S., Kheradpour, P., Ernst, J., Jordan, G., Mauceli, E., et al. (2011). A high-resolution map of human evolutionary constraint using 29 mammals. Nature *478*, 476–482. https://doi.org/10.1038/nature10530.

196. Bolger, A.M., Lohse, M., and Usadel, B. (2014). Trimmomatic: a flexible trimmer for Illumina sequence data. Bioinformatics *30*, 2114–2120. https://doi.org/10.1093/bioinformatics/btu170.

197. Cheng, H., Concepcion, G.T., Feng, X., Zhang, H., and Li, H. (2021). Haplotype-resolved de novo assembly using phased assembly graphs with hifiasm. Nat. Methods *18*, 170–175. https://doi.org/10.1038/s41592-020-01056-5.

198. Cheng, H., Jarvis, E.D., Fedrigo, O., Koepfli, K.-P., Urban, L., Gemmell, N.J., and Li, H. (2022). Haplotype-resolved assembly of diploid genomes without parental data. Nat. Biotechnol. *40*, 1332–1335. https://doi.org/10.1038/s41587-022-01261-x.

199. Zhou, C., McCarthy, S.A., and Durbin, R. (2023). YaHS: yet another Hi-C scaffolding tool. Bioinformatics *39*. https://doi.org/10.1093/bioinformatics/btac808.

200. Li, H., and Durbin, R. (2009). Fast and accurate short read alignment with Burrows-Wheeler transform. Bioinformatics *25*, 1754–1760. https://doi.org/10.1093/bioinformatics/btp324.

201. Li, H., and Durbin, R. (2010). Fast and accurate long-read alignment with Burrows-Wheeler transform. Bioinformatics *26*, 589–595. https://doi.org/10.1093/bioinformatics/btp698.

202. Open2C, Abdennur, N., Fudenberg, G., Flyamer, I.M., Galitsyna, A.A., Goloborodko, A., Imakaev, M., and Venev, S.V. (2024). Pairtools: From sequencing data to chromosome contacts. PLoS Comput. Biol. *20*, e1012164. https://doi.org/10.1371/journal.pcbi.1012164.

203. Danecek, P., Bonfield, J.K., Liddle, J., Marshall, J., Ohan, V., Pollard, M.O., Whitwham, A., Keane, T., McCarthy, S.A., Davies, R.M., et al. (2021). Twelve years of SAMtools and BCFtools. Gigascience *10*. https://doi.org/10.1093/gigascience/giab008.

204. Harry, E. (2022). PretextView (Paired REad TEXTure Viewer): A desktop application for viewing pretext contact maps.

205. Rapid curation GitLab. https://gitlab.com/wtsi-grit/rapid-curation.

206. Uliano-Silva, M., Ferreira, J.G.R.N., Krasheninnikova, K., Darwin Tree of Life Consortium, Formenti, G., Abueg, L., Torrance, J., Myers, E.W., Durbin, R., Blaxter, M., et al. (2023). MitoHiFi: a python pipeline for mitochondrial genome assembly from PacBio high fidelity reads. BMC Bioinformatics *24*, 288. https://doi.org/10.1186/s12859-023-05385-y.

207. Palmer, J.M., and Stajich, J.E. (2023). funannotate: Eukaryotic Genome Annotation Pipeline (Github).

208. Smit, A.F.A., Hubley, R., and Green, P. (2015). RepeatMasker Open-4.0. 2013--2015. Preprint at Seattle, USA.

209. Zoonomia Consortium (2020). A comparative genomics multitool for scientific discovery and conservation. Nature *587*, 240–245. https://doi.org/10.1038/s41586-020-2876-6.

210. Flynn, J.M., Hubley, R., Goubert, C., Rosen, J., Clark, A.G., Feschotte, C., and Smit, A.F. (2020). RepeatModeler2 for automated genomic discovery of transposable element families. Proc. Natl. Acad. Sci. U. S. A. *117*, 9451–9457. https://doi.org/10.1073/pnas.1921046117.

211. Išerić, H., Alkan, C., Hach, F., and Numanagić, I. (2022). Fast characterization of segmental duplication structure in multiple genome assemblies. Algorithms Mol. Biol.

212. Brown, M., González De la Rosa, P.M., and Mark, B. (2023). A Telomere Identification Toolkit https://doi.org/10.5281/zenodo.10091385.

213. Li, H. (2021). New strategies to improve minimap2 alignment accuracy. Bioinformatics.

214. Goel, M., and Schneeberger, K. (2022). plotsr: visualizing structural similarities and rearrangements between multiple genomes. Bioinformatics *38*, 2922–2926. https://doi.org/10.1093/bioinformatics/btac196.

215. Palmer, J.M., and Stajich, J. (2020). Funannotate v1.8.1: Eukaryotic genome annotation (Zenodo) https://doi.org/10.5281/ZENODO.4054262.

216. Leinonen, R., Diez, F.G., Binns, D., Fleischmann, W., Lopez, R., and Apweiler, R. (2004). UniProt archive. Bioinformatics *20*, 3236–3237. https://doi.org/10.1093/bioinformatics/bth191.

217. Haas, B.J., Papanicolaou, A., Yassour, M., Grabherr, M., Blood, P.D., Bowden, J., and Others (2013). De novo transcript sequence reconstruction from RNA Seq: reference generation and analysis with Trinity. Nat Protol. 2013; 8 (8): 1494--512. Preprint.

218. Korf, I. (2004). Gene finding in novel genomes. BMC Bioinformatics *5*, 59. https://doi.org/10.1186/1471-2105-5-59.

219. Majoros, W.H., Pertea, M., and Salzberg, S.L. (2004). TigrScan and GlimmerHMM: two open source ab initio eukaryotic gene-finders. Bioinformatics *20*, 2878–2879. https://doi.org/10.1093/bioinformatics/bth315.

220. Stanke, M., Keller, O., Gunduz, I., Hayes, A., Waack, S., and Morgenstern, B. (2006). AUGUSTUS: ab initio prediction of alternative transcripts. Nucleic Acids Res. *34*, W435–W439. https://doi.org/10.1093/nar/gkl200.

221. Haas, B.J., Salzberg, S.L., Zhu, W., Pertea, M., and Allen, J.E. (2008). Automated eukaryotic gene structure annotation using EVidenceModeler and the Program to Assemble Spliced Alignments. Genome Biol.

222. Quintaje, S.B., and Orchard, S. (2008). The annotation of both human and mouse kinomes in UniProtKB/Swiss-Prot: one small step in manual annotation, one giant leap for full comprehension of genomes. Mol. Cell. Proteomics.

223. Buchfink, B., Reuter, K., and Drost, H.-G. (2021). Sensitive protein alignments at tree-of-life scale using DIAMOND. Nat. Methods *18*, 366–368. https://doi.org/10.1038/s41592-021-01101-x.

224. Emms, D.M., and Kelly, S. (2019). OrthoFinder: phylogenetic orthology inference for comparative genomics. Genome Biol. *20*, 238. https://doi.org/10.1186/s13059-019-1832-y.

225. Ranwez, V., Douzery, E.J.P., Cambon, C., Chantret, N., and Delsuc, F. (2018). MACSE v2: Toolkit for the Alignment of Coding Sequences Accounting for Frameshifts and Stop Codons. Mol. Biol. Evol. *35*, 2582–2584. https://doi.org/10.1093/molbev/msy159.

226. Whelan, S., Irisarri, I., and Burki, F. (2018). PREQUAL: detecting non-homologous characters in sets of unaligned homologous sequences. Bioinformatics *34*, 3929–3930. https://doi.org/10.1093/bioinformatics/bty448.

227. Bowman, J., Silva, N., Schüueftan, E., Almeida, J.M., Brattig-Correia, R., Oliveira, R.A., Tüttelmann, F., Enard, D., Navarro-Costa, P., and Lynch, V.J. (2023). Pervasive relaxed selection on spermatogenesis genes coincident with the evolution of polygyny in gorillas. bioRxiv, 2023.10.27.564379. https://doi.org/10.1101/2023.10.27.564379.

228. Scornavacca, C., Belkhir, K., Lopez, J., Dernat, R., Delsuc, F., Douzery, E.J.P., and Ranwez, V. (2019). OrthoMaM v10: Scaling-Up Orthologous Coding Sequence and Exon Alignments with More than One Hundred Mammalian Genomes. Mol. Biol. Evol. *36*, 861–862. https://doi.org/10.1093/molbev/msz015.

229. Cunningham, F., Allen, J.E., Allen, J., Alvarez-Jarreta, J., Amode, M.R., Armean, I.M., Austine-

Orimoloye, O., Azov, A.G., Barnes, I., Bennett, R., et al. (2022). Ensembl 2022. Nucleic Acids Res. *50*, D988–D995. https://doi.org/10.1093/nar/gkab1049.

230. Minh, B.Q., Schmidt, H.A., Chernomor, O., Schrempf, D., Woodhams, M.D., von Haeseler, A., and Lanfear, R. (2020). IQ-TREE 2: New Models and Efficient Methods for Phylogenetic Inference in the Genomic Era. Mol. Biol. Evol. *37*, 1530–1534. https://doi.org/10.1093/molbev/msaa015.

231. Dos Reis, M., and Yang, Z. (2019). Bayesian Molecular Clock Dating Using Genome-Scale Datasets. Methods Mol. Biol. *1910*, 309–330. https://doi.org/10.1007/978-1-4939-9074-0_10.

232. Phillips, M.J. (2016). Geomolecular dating and the origin of placental mammals. Syst. Biol. *65*, 546–557. https://doi.org/10.1093/sysbio/syv115.

233. Gunnell, G.F., and Simmons, N.B. (2005). Fossil evidence and the origin of bats. J. Mamm. Evol. *12*, 209–246. https://doi.org/10.1007/s10914-005-6945-2.

234. Eiting, T.P., and Gunnell, G.F. (2009). Global Completeness of the Bat Fossil Record. J. Mamm. Evol. *16*, 151–173. https://doi.org/10.1007/s10914-009-9118-x.

235. Storch, G., Sigé, B., and Habersetzer, J. (2002). Tachypteron franzeni n. gen., n. sp., earliest emballonurid bat from the Middle Eocene of Messel (Mammalia, Chiroptera). Palaontol. Z. *76*, 189–199. https://doi.org/10.1007/bf02989856.

236. Ravel, A., Marivaux, L., Tabuce, R., Ben Haj Ali, M., Essid, E.L.M., and Vianey-Liaud, M. (2012). A new large philisid (Mammalia, Chiroptera, Vespertilionoidea) from the late Early Eocene of Chambi, Tunisia: LARGE BAT FROM CHAMBI. Palaeontology *55*, 1035–1041. https://doi.org/10.1111/j.1475-4983.2012.01160.x.

237. Lim, B.K. (2009). Review of the origins and biogeography of bats in South America. Chiroptera Neotropical *15*, 391–410.

238. Morgan, G.S., and Czaplewski, N.J. (2003). A New Bat (Chiroptera: Natalidae) from the Early Miocene of Florida, with Comments on Natalid Phylogeny. J Mammal *84*, 729–752. https://doi.org/10.1644/1545-1542(2003)084<0729:ANBCNF>2.0.CO;2.

239. Foley, N.M., Mason, V.C., Harris, A.J., Bredemeyer, K.R., Damas, J., Lewin, H.A., Eizirik, E., Gatesy, J., Karlsson, E.K., Lindblad-Toh, K., et al. (2023). A genomic timescale for placental mammal evolution. Science *380*, eabl8189. https://doi.org/10.1126/science.abl8189.

240. Elliot, M.G., and Mooers, A.Ø. (2014). Inferring ancestral states without assuming neutrality or gradualism using a stable model of continuous character evolution. BMC Evol. Biol. *14*, 226. https://doi.org/10.1186/s12862-014-0226-8.

241. Kosakovsky Pond, S.L., Poon, A.F.Y., Velazquez, R., Weaver, S., Hepler, N.L., Murrell, B., Shank, S.D., Magalis, B.R., Bouvier, D., Nekrutenko, A., et al. (2020). HyPhy 2.5-A customizable platform for evolutionary hypothesis testing using PHYlogenies. Mol. Biol. Evol. *37*, 295–299. https://doi.org/10.1093/molbev/msz197.

242. Lucaci, A.G., Zehr, J.D., Enard, D., Thornton, J.W., and Kosakovsky Pond, S.L. (2023). Evolutionary Shortcuts via Multinucleotide Substitutions and Their Impact on Natural Selection Analyses. Mol. Biol. Evol. *40*. https://doi.org/10.1093/molbev/msad150.

243. Wu, N., Nguyen, X.-N., Wang, L., Appourchaux, R., Zhang, C., Panthu, B., Gruffat, H., Journo, C., Alais, S., Qin, J., et al. (2019). The interferon stimulated gene 20 protein (ISG20) is an innate

defense antiviral factor that discriminates self versus non-self translation. PLoS Pathog. *15*. https://doi.org/10.1371/journal.ppat.1008093.

244. GTEx Consortium (2020). The GTEx Consortium atlas of genetic regulatory effects across human tissues. Science *369*, 1318–1330. https://doi.org/10.1126/science.aaz1776.

245. Luisi, P., Alvarez-Ponce, D., Pybus, M., Fares, M.A., Bertranpetit, J., and Laayouni, H. (2015). Recent positive selection has acted on genes encoding proteins with more interactions within the whole human interactome. Genome Biol. Evol. *7*, 1141–1154. https://doi.org/10.1093/gbe/evv055.

246. Gene Ontology Consortium (2021). The Gene Ontology resource: enriching a GOld mine. Nucleic Acids Res. *49*, D325–D334. https://doi.org/10.1093/nar/gkaa1113.

247. Eisenberg, E., and Levanon, E.Y. (2013). Human housekeeping genes, revisited. Trends Genet. *29*, 569–574. https://doi.org/10.1016/j.tig.2013.05.010.

248. Kosakovsky Pond, S.L., Murrell, B., Fourment, M., Frost, S.D.W., Delport, W., and Scheffler, K. (2011). A random effects branch-site model for detecting episodic diversifying selection. Mol. Biol. Evol. *28*, 3033–3043. https://doi.org/10.1093/molbev/msr125.

249. Quinlan, A.R. (2014). BEDTools: The Swiss-Army Tool for Genome Feature Analysis. Curr. Protoc. Bioinformatics *47*, 11.12.1–34. https://doi.org/10.1002/0471250953.bi1112s47.

250. Dainat, J. AGAT: Another Gff Analysis Toolkit to handle annotations in any GTF/GFF format https://doi.org/10.5281/zenodo.3552717.

251. Legrand, A., Dahoui, C., De La Myre Mory, C., Noy, K., Guiguettaz, L., Versapuech, M., Loyer, C., Pillon, M., Wcislo, M., Guéguen, L., et al. (2024). SAMD9L acts as an antiviral factor against HIV-1 and primate lentiviruses by restricting viral and cellular translation. PLoS Biol. *22*, e3002696. https://doi.org/10.1371/journal.pbio.3002696.

252. Gene Ontology Consortium, Aleksander, S.A., Balhoff, J., Carbon, S., Cherry, J.M., Drabkin, H.J., Ebert, D., Feuermann, M., Gaudet, P., Harris, N.L., et al. (2023). The Gene Ontology knowledgebase in 2023. Genetics *224*, iyad031. https://doi.org/10.1093/genetics/iyad031.

253. Ashburner, M., Ball, C.A., Blake, J.A., Botstein, D., Butler, H., Cherry, J.M., Davis, A.P., Dolinski, K., Dwight, S.S., Eppig, J.T., et al. (2000). Gene ontology: tool for the unification of biology. The Gene Ontology Consortium. Nat. Genet. *25*, 25–29. https://doi.org/10.1038/75556.

254. Kanehisa, M., and Goto, S. (2000). KEGG: kyoto encyclopedia of genes and genomes. Nucleic Acids Res. *28*, 27–30. https://doi.org/10.1093/nar/28.1.27.

255. Kowalczyk, A., Partha, R., Clark, N.L., and Chikina, M. (2020). Pan-mammalian analysis of molecular constraints underlying extended lifespan. Elife *9*. https://doi.org/10.7554/eLife.51089.

Materials and Methods

Data availability

All sequencing data and genomes generated in this study are available on NCBI under Bioprojects PRJNA973719 and PRJNA1035541. Annotations generated in this study are available at

https://github.com/docmanny/myotis-gene-annotations. All other code is available at https://github.com/sudmantlab/MyotisGenomeAssembly.

Sample collection and cell line derivation

All bats sampled for this study were wild caught under scientific collection permits for California and Arizona (see Supplemental Table 1). Bats were sampled using standard mist-netting procedures, including taking standard body measurements, following USGS recommendations for White-Nose Syndrome and COVID-19 prevention[192,193].

For *M. lucifugus*, the donor individual was field-caught in California and transported to the Genetics Laboratory of the California Department of Fish and Wildlife, where they were euthanized via isofluorane. The *M. velifer* individual was caught in Arizona and euthanized in the field via isoflurane. For both *M. lucifugus* and *M. velifer*, tissues were collected and preserved via flash-freezing in liquid nitrogen.

For *M. volans, M. occultus, M. auriculus,* and *M. californicus*, two 3-mm wing punch biopsies were taken from the left and right plagiopatagium of each donor individual and placed in a live cell collection media consisting of DMEM/F12 (Gibco) supplemented with 15mM HEPES (Gibco), 20% FBS (Gibco), and 0.2% Primocin (Invivogen) [@yohe2019; @curty2023; @capel2023]. Wing punches were then brought back to a cell culture facility in Berkeley, where they were used to generate cell lines as previously described[@yohe2019; @curty2023; @capel2023]. Additional cell lines for *M. lucifugus, M. velifer, M. yumanensis, M. evotis,* and *M. thysanodes* were similarly collected and generated.

Cell lines for the *M. evotis* and *M. thysanodes* genomes were generously provided by Richard Miller. Cell lines for functional work in *Rousettus langosus*, *Pteropus rodrigensis*, and *Eidolon helvum* were provided by the San Diego Frozen Zoo.

Sequencing and assembly

For 6 genomes (*M. evotis, M. thysanodes, M. volans, M. occultus, M. auriculus,* and *M. californicus*) DNA was extracted from primary cell lines expanded from 3M cells at Passage 2-4 to approximately 40M cells per line using a Circulomics BigDNA CCB kit following the UHMW protocol for cells. DNA from *M. lucifugus* was extracted from flash-frozen tissue by the Genetics Lab of the California Department of Fish and Wildlife. PacBio HiFi libraries were generated and sequenced on a Sequel II (PacBio) by the Functional Genomics Core at the University of California, Berkeley. For cell-line-derived genomes, Hi-C libraries for these genomes were generated from 1M cells at Passage 3 using the OmniC for Illumina kit (Dovetail genomics); libraries were submitted for quality control and sequencing on the Illumina NovaSeq platform (Novogene). For the *M. velifer* genomes, DNA was extracted from flash-frozen tissues, and all DNA extraction, library prep, and sequencing was completed by Dovetail Genomics following standard protocols. For *M. lucifugus*, a previously published Hi-C dataset from 4 pooled individuals was used for scaffolding[194,195].

The PacBio reads were processed using SMRTTools (v6.0.0-1, PacBio) to generate the circular consensus sequences using the settings --minPasses=3 --minRQ=0.99. Hi-C reads were processed using trimmomatic[196] (v0.35-6) to remove adapter sequences and low-quality bases using the settings ILLUMINACLIP:data/trimmomatic-adapters/TruSeq3-PE-2.fa:2:40:15 SLIDINGWINDOW:5:20. To generate the primary contig assemblies, we used hifiasm[197,198] (v0.14-hd174df1_0) in Hi-C mode, providing both the CCS

reads and the trimmed Hi-C reads as input, and purging duplicates using the -l2 option. For our reference genomes, we proceeded with the primary contig assembly (*.asm.hic.p_ctg.gfa).

All reference genomes were scaffolded with YAHS[199] (v1.1a.1s) and the Hi-C datasets. Dovetail Omni-C data were processed and mapped to the genome following the manufacturer's instructions using bwa[200,201] (v0.7.17-h5bf99c6_8), pairtools[202] (v0.3.0-py37hb9c2fc3_5), and samtools[203] (v1.12-h9aed4be_1). YAHS was run using both default settings as well as with --no-contig-ec; after comparing the outputs, we proceeded with the --no-contig-ec version for our final assemblies.

To finalize the assemblies, we performed manual curation using PreTextView[204] and the Rapid Curation toolkit[205] (version ff964069). The X chromosomes were identified based on size, synteny across genomes, and half-coverage observed in XY genomes; putative Y chromosomes were similarly identified in XY genomes. Mitochondrial genomes were identified and removed from the final assembly by running mitohifi[206] (v3.0) in contig mode on the assembly and removing all scaffolds identified as mitogenomes. The consensus mitogenome from mitohifi was designated as the representative mitogenome for the assembly after manual curation. Finally, to eliminate spurious duplicates, we used FunAnnotate[207] (v1.8.15) and the “clean” function to identify and remove any remaining scaffolds with 90% identical to a larger scaffold.

Identification and annotation of repetitive elements

We used RepeatMasker[208] (version 4.0.7-open) to annotate repetitive elements in our genomes. We first ran RepeatMasker using a curated database of transposable elements from 249 mammalian species[36,209] (David Ray, pers. comm.) and the settings “*-engine ncbi -s -noisy -xsmall*” followed by a second run using RepeatModeler[210] and RepeatMasker to identify *de novo* repeats missing from the curated database. All repeats were then soft-masked in all genomes. To assess the repeat landscape, we calculated the summary of divergence from the repeat alignments and created the repeat landscape using auxiliary RepeatMasker scripts (calcDivergenceFromAlign.pl & createRepeatLandscape.pl).

Structural variation

To understand the distribution of structural variants, including segmental duplication events, we used SyRI (Senteny and Rearrangement Identifier[128]) and BISER (Brisk Inference of Segmental duplication Evolutionary stRucture[211]). We first masked telomere regions using TIDK (Telomere Identification toolKit[212]), and mapped the primary 22 scaffolds of the nearctic *Myotis* genomes to each other with minimap2[213]. The scaffold corresponding to the X chromosome was omitted because there is no corresponding scaffold in the *M. yumanensis* assembly. To verify homologous chromosomes and fix strand orientation, we used *fixchr* from the SyRI package and manually renamed scaffolds accordingly, then re-mapped with minimap2. We ran SyRI on the resulting files and plotted the results with plotsr[214]. We ran BISER on the primary 22 scaffolds of the nearctic *Myotis* genomes with –keep-contigs and default settings to generate bed files with the inferred segmental duplication regions.

RNA-seq

To assist our annotation efforts, we generated mRNA-seq for 7 of the species sequenced *de novo* in this study. For *M. velifer*, samples of heart, brain, kidneys, lungs, pancreas, and testis collected from the donor individual were provided to Dovetail Genomics (CA, USA) for mRNA-seq library preparation and sequencing. Using the same cell lines used for the genomes of *M. occultus, M. thysanodes, M. evotis, M. volans, M. auriculus,* and *M. californicus*, we generated rRNA-depleted total RNA-seq libraries using the NEBNext rRNA Depletion Kit v2 and Ultra II Directional RNA Library Prep Kits. RNA and libraries were quality controlled on an Agillent Bioanalyzer using the RNA 6000 Nano and DNA High Sensitivity assays, respectively. Samples were sequenced on to 100M 150PE reads per sample using the Novoseq platform (Novogene). For *M. lucifugus*, we used the following published RNA-seq data on NCBI SRA generated using poly-A selection and paired-end sequencing: SRR6793287, SRR6793288, SRR6793289, SRR6793290, SRR6793291, SRR6793292, SRR6793293, SRR6793294, SRR6793295, SRR6793296, SRR6793297, SRR6793298, SRR6793299, SRR6793300, SRR6793301, SRR7064951, SRR10512805, SRR10512806, SRR10512807, SRR10512808, SRR10512809, SRR10512818, SRR10512829, SRR10512840, SRR10512845, SRR10512846, SRR10512847, SRR10512848, SRR10512849, SRR10512850, SRR10512851, SRR10512852, SRR10083333, SRR10083334, SRR10083335, SRR10083336, SRR10083337, SRR10083338, SRR10083339, SRR10083340, SRR10083351, SRR10083352, SRR1916825, SRR1916826, SRR1916827, SRR1916830, SRR1916832, SRR1916834, SRR1916836, SRR1916839, SRR1916841, SRR1916842, SRR18761564, SRR18761566, SRR18761568, SRR18761571, SRR18761573, SRR18761563, SRR18761565, SRR18761567, SRR18761569, SRR18761570, SRR18761572, SRR18761574, SRR1270869, SRR1270914, SRR1270919, SRR1270921, SRR1270922, SRR1270923, SRR4249979, SRR4249988, SRR5676382, SRR5676383, SRR5676395, SRR5676396, SRR5676402, SRR1869462, and SRR1013468.

Gene annotation and alignment

Gene predictions

To create optimal gene annotations, we combined *ab initio* gene predictions; orthology inferences; and transcriptomic evidence for a total-evidence dataset facilitated using FunAnnotate[207,215] with manual interventions. To generate high-quality orthology-based evidence, we downloaded the UNIPARC database[216] of genes present in all Chiropteran genomes and mapped these proteins to our genomes using miniprot[62] (v 0.6-r194-dirty). We assembled our transcriptome data into transcripts using TRINITY[217] (v 2.13.2), and mapped these transcripts to our genomes using minimap2[213] (v 2.24).

Next, we ran BUSCO[63,64] (version 5.4.3) using the “eutheria_odb10” database and AUGUSTUS[58] to identify BUSCO orthologs in our genomes. GFFs describing the gene structure of single-copy BUSCO orthologs was then used by FunAnnotate to train SNAP[218] and GlimmerHMM[219] (v 3.0.4) prior to gene prediction. GeneMark-ES[59] (v 4.72) was run using its self-trained model. AUGUSTUS[220] (v 3.4) was run using a previously-generated model jointly trained on 6 high-quality bat genome assemblies[36] and supplemented with protein and transcriptome hints generated by FunAnnotate from the UNIPARC and Trinity datasets.

To leverage high-quality annotations from other genomes, we used TOGA[61] (version 1.0.1) to generate gene annotations for each of our species, using inference from hg38 annotations. TOGA outputs a table of genes (“reg” genes) associated with the projected transcripts from the reference genomes, and a BED file describing the CDS structure of these projected transcripts. To generate a final GFF file summarizing these data, we converted the original BED file to a GFF file using [program]; removed the erroneous “Gene” level attributes; and

added in new “Gene” entries describing the TOGA-designated genes, modifying the “Parent” attributes of the mRNAs to refer to the correct parent gene. Transcript projections that were not associated with a TOGA gene designation were then dropped.

Finally, we used LiftOff[60] (v1.6.3) to lift over annotations from the *Myotis myotis* genome (mMyoMyo1.0_primary[36]). Using BUSCO and manual curation, we assessed both the original GenBank (GCF_014108235.1) and NCBI RefSeq (GCA_014108235.1) annotations, and selected the NCBI RefSeq annotation, as it had slightly improved BUSCO scoring and less erroneous intron-exon junctions at select genes. We removed all non-protein-coding genes from the initial GFF file, then ran LiftOff using the settings “ -exclude_partial -polish -cds”.

We evaluated each line of evidence by assessing their completeness using BUSCO and comparing the completeness score to the total number of predicted genes. We found that SNAP and GLIMMERHMM performed the poorest for gene annotations, with both the lowest BUSCO scores and the highest number of low-quality predictions. The miniprot-UniParc and TOGA-hg38 datasets generated the highest quality gene prediction datasets, with near-complete BUSCO scores and reduced low-quality protein predictions.

Gene prediction curation

We used EvidenceModeler[221] (version 2.0) to generate an initial consensus gene set using only the best lines of evidence (AUGUSTUS, weight 2; high quality AUGUSTUS, weight 5; TOGA-hg38, weight 12; miniprot-UniParc, weight 5; and LiftOff-mMyoMyo1, weight 5) with hints from protein orthology (miniprot-UniParc, weight 6) and RNA-seq (TRINITY, weight 5) for alternative splicing. By default, EvidenceModeler does not consider genes that are located within intronic regions of other genes. To restore these genes, we intersected the EvidenceModeler consensus gene GFF with the TOGA-hg38 GFF to identify which genes were present in intronic regions and omitted from EvidenceModeler; these genes were then added back to the EvidenceModeler gene set.

To eliminate remaining spurious predictions, we cross-referenced our gene annotations against the SwissProt[222] database using DIAMOND[223] (v. 2.1.4) with settings “*--ultra-sensitive --outfmt 6 qseqid bitscore sseqid pident length mismatch gapopen qlen qstart qend slen sstart send ppos evalue --max-target-seqs 1 --evalue 1e-10* ”. We kept all genes that matched a protein on SwissProt with at least 80% identity, matched over 50% of the target sequence, and coded for at least 50 amino acids. Of the remaining genes, we kept them only if they contained both a start and stop codon with no internal stop codons.

Finally, we further curated our annotations by putting the EVM and TOGA gene predictions in competition with each other when they both annotated the same locus, but with different overlapping or neighboring annotations. In such cases, one of the gene annotations is likely closer to the truth. To determine which, we compared EVM and TOGA gene models with their closest human gene BLAST hits. Only proteins with a BLAST match to a human Ensembl v99 annotation with the lowest E-values below 0.001 were considered. These human homologs were used as a reference for curation as they are well-defined and characterized. We observed that occasionally, either the EVM or TOGA model predicted a transcript much longer than their human closest homolog. Closer inspection revealed that such cases represent artifactual mergers of neighboring genes during the annotation process, clearly visible from the fact that they map to two distinct human homologs in succession. Such cases were resolved by choosing the annotations (between EVM and TOGA) that were not affected by the artificial merger. We further observed a specific class of mergers between neighboring, segmentally duplicated

genes, with the resulting annotations representing chimeric mixes of exons from the duplicates. In such cases we selected the annotations that clearly stayed within the boundaries of the separate duplicates, as identified by mapping to the closest human homolog. For the remaining annotations where both TOGA and EVM both mapped to a single human homolog throughout their entire length, we selected the most complete annotation that was closest in length to the human homolog.

Orthologous Gene Alignments

Phylogeny and selection analyses described in this manuscript rely on high-quality alignments of bat orthologous coding sequences. To first find and align orthologous *Myotis* genes to the greatest extent possible, we first complemented the gene annotations described above with likely missing annotations that could still be found through BLAT homology searches. Missing gene annotations are always expected in non-model species genomes and reflect a feature of annotation pipelines in general, not an artifactual issue. For example if the first coding exon of a gene falls into a small local assembly gap, the lack of a start codon may prevent the trigger of a CDS annotation, or may lead to the clearly incomplete CDS being subsequently filtered out. Similarly, erroneous indels representing sequencing errors may interrupt coding reading frames. Genes with missing annotations can still be detected in assemblies through classic BLAST or BLAT homology searches, and then aligned with their annotated orthologs from other species. To align orthologous *Myotis* genes from ten species (those sequenced here plus *Myotis myotis* and *M. yumanensis*), we first decided to use *Myotis velifer* as the *Myotis* species of reference, since the RNA-seq data we used was generated with *M. velifer* tissues.

We first looked for missing homologs of *M. velifer* genes in the other *Myotis* genomes by blatting *M. velifer* CDS to the other *Myotis* assemblies (BLAT command line including non-default options -q=dnax -t=dnax -fine) to find matches outside of already annotated genomic segments. When multiple velifer CDS matched to the same locus with multiple overlapping homologous BLAT matches, we selected the match with the highest number of identical nucleotides. The remaining matching BLAT sequences were further considered if they spanned at least 50% of the velifer CDS, and included 100 codons or more. BLAT matches including stop codons were removed. This process added 1,837 putative CDS to consider for orthologous alignments for *M. auriculus*, 1,785 for *M. californicus*, 1,796 for *M. evotis*, 1,505 for *M. lucifugus*, 3,234 for *M. myotis*, 1,826 for *M. occultus*, 1,822 for *M. thysanodes*, 1,800 for *M. volans* and 1,729 for *M. yumanensis*. The correct reading frames for these putative CDS were then determined by aligning to the velifer CDS that generated the initial match with MACSE v2. MACSE has the crucial advantage over other aligners of being able to repair broken reading frames due to sequencing indel errors or erroneous gene annotations. At this stage, we restricted any further analysis to those velifer CDS with human homologs (BLASTP E-value<0.001 with at least one human canonical protein-coding gene from Ensembl). One-to-one orthologs with the 23,030 remaining velifer CDS in other *Myotis* species were then determined using Orthofinder v2.5.4[224]. The sequences of each group of ortholog were then aligned with MACSE v2[225] with default settings. The resulting CDS with potentially repaired reading frames were then checked with PREQUAL[226] to exclude sequencing errors and erroneous inclusion of non-homologous segments in annotations. The remaining parts of orthologous sequences that passed PREQUAL filtering were then aligned again using MACSE v2 with default settings. The first round of alignment with MACSE ensures that we do not remove portions of CDS that look like they have no homology and would thus be removed by PREQUAL, just because of frameshifts that are easy to repair first with MACSE. The second round of MACSE is to align the remaining codons once PREQUAL has removed erroneous portions of CDS that could have otherwise disturbed the alignment process. We further masked (i.e. replaced with indels) codons near indels with putative alignment errors as described in Bowman et al.[227]. Of the 23,030 initial *M. velifer* CDSs, this process resulted in 21,756 alignments with at least one ortholog in another *Myotis* species.

We also aligned pan-Chiroptera orthologs from 47 non-*Myotis* genomes publicly available on NCBI at the time of analysis, to test the generality of our observations to all bats. We used the same strategy described above to complement *Myotis* gene annotations with BLAT matches, but this time blatting velifer CDS on non-Myotis assemblies (with -q=dnax -t=dnax -fine again) to find all the potential orthologs in the non-Myotis assemblies. We previously found that because BLAT represents a first filter to include only portions of homologous CDS with good local similarity, using BLAT matches results in higher quality alignments of orthologs than using existing gene annotations of disparate qualities that too often include non-homologous portions of introns among other issues[227,228]. As before with only *Myotis* species, we recovered putative one-to-one orthologs with Orthofinder. This process resulted in the alignment (as previously described with two rounds of MACSE and PREQUAL in the middle) of 19,009 orthologous CDS with at least one non-*Myotis* orthologous CDS.

To test whether the patterns of virus-driven adaptation observed in bats are unique across mammals, we also prepared four more datasets of 70 primate orthologous CDS alignments, 138 euungulate alignments, 127 glire alignments, and 82 carnivora alignments (see supplementary files XY for the species and their respective assemblies used). We used the same pipeline as the one used to align 47 pan-chiroptera species as described above, except that instead of starting from velifer CDS, we started from human Ensembl v109[229] CDS (the longest isoform available in each case) for primates, *Mus musculus* Ensembl v109 longest CDS for glires, *Canis familiaris* Ensembl v109 longest CDS for carnivores, and *Bos taurus* Ensembl v109 longest CDS for euungulates . These species were chosen for the very high quality of their gene annotations.

Gene Trees & Phylogeny

A phylogeny of all 536 mammals in our alignments was generated using IQTREE[230] (version 2.3.1) using all gene alignments with the settings "-B 1000 -m GTR+F3x4+R6." To generate gene trees, we first filtered our gene alignments to exclude alignments with over 50% gaps in the sequence and less than 4 species. With the remaining alignments, we used IQTREE to find the best-fitting substitution model and tree using settings "--wbtl --bnni --alrt 1000 -B 1000 --safe". The best substitution models for each gene were saved as a NEXUS file. To generate the phylogeny of bats, we first concatenated all gene alignments using `catfasta2phyml` (https://github.com/nylander/catfasta2phyml) to concatenate our individual gene alignments into species-level alignments, filling in missing species in each sub-alignment with gap symbols to preserve the alignment structure. Furthermore, we generated a partition file describing the region of each gene sub-alignment within the concatenated alignment.

Time-calibration of 59 bat genomes

Using our codon alignments of 59 bat genomes, we generated a time-calibrated phylogeny using mcmctree[231] and PAML[72] (v. 4.10.0) using an approximate likelihood method. Using the pan-bat codon alignments and our phylogeny as input, with fossil calibrations based on previously published work[4,36,232–239], we ran *mcmctree* twice to generate the Hessian matrix and confirm convergence. This was followed by 10 independent chains using the "out.BV" file from the first run. Finally, the output files of all 10 chains were combined to compute final divergence time estimates (see Table S2).

Ancestral Body Size, Lifespan, and Cancer Risk reconstruction

To explore how body size and lifespan have evolved over time in mammals, we used a super-phylogeny of mammal species[67] subsampled to only contain species with extant body size and lifespan data collected from AnAge[15] and PanTHERIA[16]. Ancestral body sizes and lifespans were simulated separately using StableTraits[240].

To estimate ancestral longevity quotients (AncLQs), we followed the method of Austad and Fisher[18] and used a linear model of lifespan given body size trained on non-flying mammals to predict the lifespans at each ancestral node given median estimates of body size. AncLQs were then estimated from the ratio of observed lifespan versus predicted lifespan for each node.

Relative Incidence of Cancer Risk (RICR) was calculated across our mammalian phylogeny following the method of Vazquez and Lynch (2021)[46]. The cancer risk *K* at a given node was calculated using the log of the median predicted body size and lifespan. An organism's lifetime risk of cancer *K* is proportional to Dt^6, where D is the body size and T is the maximum lifespan. RICR is then calculated as the $\log_2$ ratio of the cancer risk between a node and its direct ancestor.

Selection Scans & Evolutionary Rates

aBSREL

To conservatively test for branch-specific selection, we used aBSREL[98,241] (version 2.5.48) to test for selection at each branch within the Nearctic *Myotis* clade for 15,734 gene alignments spanning 536 mammals. These genes were identified as 1:1 orthologs across the full alignment, with no more than 50% sequence gaps and at least 4 species present in the alignment. We defined genes under selection as those with an FDR-corrected p-value of less than 0.05; genes were specifically identified as under positive selection if $\omega>1$.

BUSTED

To quantify the total amount of positive selection across the *Myotis* tree or the different species trees used in this manuscript, we used an improved version of the BUSTED[113,241] test called BUSTED-MH. The original BUSTED test estimates for a given gene the proportion of codons that have evolved under positive selection, with dN/dS>1, summed over all the branches of a given tree, regardless of the branch and regardless of the codons in a multi-species alignment. The version of BUSTED we used, BUSTED-MH, includes two crucial improvements over the original BUSTED that make it much less likely to generate false positive inferences of positive selection, albeit at the cost of becoming a very conservative test. First, BUSTED-MH takes synonymous substitution rate variation into account, which prevents mistaking cases where dN/dS is greater than one just because dS is low, with cases where dN/dS is greater than one because positive selection actually increased dN. Second, BUSTED-MH takes complex substitutions that simultaneously involve more than one nucleotide into account in its likelihood models. This prevents attributing positive selection to cases where dN/dS is greater than one where instead a complex substitution changed multiple amino acids in a single event. BUSTED-MH has been shown to strongly reduce the rate of false positives that typically plague dN/dS-based tests of positive selection[242].

We applied BUSTED-MH to 19,646 *Myotis* orthologous CDS alignments with at least five orthologs. These orthologs are cases where the Orthofinder gene trees coincide with the species tree. This effectively removes issues regarding whether we should use the gene or the species tree, at the cost of removing 2,110 genes from the *Myotis* selection analysis. Similarly, we applied BUSTED-MH to 17,469 non-*Myotis* bat alignments with at least five orthologs. This includes a subset of 14,091 alignments with orthologs in two thirds of the non-*Myotis* bat species that we specifically used to show that patterns of virus-driven adaptation are representative of all, and not just a limited subset of bats. We also tested 17,890 primate alignments with at least five orthologs with BUSTED-MH, as well as 19,311 glire, 18,000 carnivora and 18,504 ungulate alignments.

RERConverge

Between-species life history diversity may be undergirded by significant evolutionary rate shifts in important genes, where evolutionary change across the gene tree correlates either positively or negatively with changes in a particular life history trait across the trait tree. In *Myotis*, we were interested specifically in testing whether or not longevity-related metrics could be correlated with evolutionary rate shifts for particular genes, and if, among those, we could identify types of genes (gene ontologies) that were enriched.

To answer this question, we used RERconverge[109], an R package which uses gene trees to compute relative evolutionary rates (RERs), then tests for correlations between RERs and trait changes between species. 40 bat genomes were aligned to produce MSAs, which were then split into three groups to be tested independently: all bats (n=59), non-Myotis bats (n=29), and Myotis (n=11). Gene trees were constructed under the GTR+G model with the same topology as determined in our phylogenetic analysis, across all 39 available bat species. After concatenating the gene trees, RERs were calculated in RERconverge. Trait correlation analysis was performed by regressing these RERs against 4 distinct trait axes. Two of the axes were maximum longevity and size, which were obtained from AnAge[154] and PanTHERIA[16]; an additional two axes were obtained by plotting species along the first 2 principal components of size and maximum longevity. Since size generally correlates with longevity, even within Myotis, PCA allows us to describe species using orthogonal trait axes that roughly correspond to size-independent longevity and longevity-independent size. Using a Wilcoxon rank-sum test, we then tested for enrichment in correlation significance amongst different gene sets.

RELAX

The evolution of life history diversity across a clade may also manifest in differential selection regimes across relevant genes or types of genes. Specifically, the evolution of a particular life history may be driven by either relaxation or intensification of selection in different genes. In Myotis, we were again interested in whether we could identify genes and gene sets related to increased longevity within the clade.

RELAX[102] is used to identify genes under either relaxation or intensification of selection across groups groups of species within a clade using MSAs and a labeled species tree. MSAs for 11 available Myotis species across ~19,000 shared genes were fit using the BS-REL framework to a branch-site model, using the species tree determined from our phylogenetic analysis. 4 longer-lived species, *Myotis lucifugus*, *M. occultus*, *M. evotis*, and *M. myotis* were set as the foreground class with the remaining species set as the background class. RELAX then used these branch classes to estimate a distribution of ω (dN/dS) for each branch class, constrained by the relaxation factor k. An LRT is performed for $k \neq 1$ against $k = 1$, with $k > 1$ implying relaxation of selection and $k < 1$ implying intensification of selection. The results from this test were then used to perform a Wilcoxon rank-sum test to identify enrichment in the significance of the k-parameter amongst different gene sets.

VIPs

To determine if *Myotis* and other bats are enriched for adaptation at Virus Interacting Proteins (VIPs), we conducted a test comparing levels of adaptation, inferred by BUSTED, in sets of VIP genes compared to matched control genes. Sets of control genes were resampled in a bootstrap procedure (https://github.com/DavidPierreEnard/Gene_Set_Enrichment_Pipeline) to generate 95% confidence intervals for sets of genes at progressively smaller BUSTED p-value thresholds[112,114,116,155]. When VIPs are subject to greater levels of positive selection than expected relative to the sets of matched control genes, we expect a pattern in which the high p-value thresholds show weaker enrichment but smaller confidence intervals, because more genes are used in these calculations. As the p-value threshold gets smaller, the signal of enrichment is expected to get stronger but at the expense of larger confidence intervals.

We generated five sets of VIP genes: A set of all VIP genes with aligned orthologs from at least five species in the tested clade (Nearctic *Myotis* or pan-Chiroptera without *Myotis*); a set of VIP genes with known pro- and/or anti-viral activity; a set of VIP genes with no known pro- and/or anti-viral activity; a set of VIP genes that interact only with DNA viruses; and a set of VIP genes that interact only with RNA viruses. Because both the number of species and genes included, as well as their level of homology, influences the power of these tests we also tested the influence of the stringency of gene choice by generating a separate set of genes for the pan-Chiroptera analyses that included only genes with aligned orthologs in at least two thirds of the non-*Myotis* species. Analyses using this more limited set of genes show the same result in terms of enrichment of adaptation in VIP genes and comparing DNA VIPs and RNA VIPs, showing that the observed patterns are valid across bats regardless of the stringency of homology.

The bootstrap procedure matches a tested gene set of interest such as VIPs with sets of control genes (non-VIPs when testing VIPs) that have the same average values as the set of interest for multiple potential confounding factors that could explain differences in adaptation instead of interactions with viruses. For example, if the level of gene mRNA expression has an influence on the rate of adaptation, we then need to match VIPs with control sets of non-VIPs that collectively have the same average expression as VIPs. For each group of tested VIPs we build 1,000 control sets with randomly sampled non-VIPs according to a matching procedure described in Enard & Petrov 2020[155,243]. We match the 27 following factors between VIPs and non-VIPs, for all tested groups of species:

- the length of the aligned CDS.
- the overall CDS GC content in each orthologous alignment.
- the GC content at aligned codons' position 1, 2 and 3 separately.
- the number of species with a onetoone ortholog out of all the species included in an alignment, where species with no ortholog are represented by gaps the whole length of the alignment.
- the number of species with an ortholog at least 90% of the length of the species of reference (Myotis velifer in bats, human in primates, etc; see above).
- the overall proportion of each orthologous alignment made of indels.
- the three synonymous rates of evolution estimated by the likelihood model of HYPHY Busted.
- the proportions of codons that fall in the three latter synonymous rates.
- average human mRNA expression in 53 GTEx v7 tissues[244], in $\log_2$ of Transcripts Per Million (TPM).

- lymphocyte human mRNA expression from GTEx v7, in $\log_2$ of TPM.
- testis human mRNA expression from GTEx v7, in $\log_2$ of TPM.
- mRNA expression in $\log_2$ of TPM for six separate *Myotis velifer* tissues: heart, brain, kidneys, lungs, pancreas, and testis.
- the number in $\log_2$ of protein-protein interactions (PPIs) in the human protein interaction network[245].
- the proportion of genes that are immune genes according to Gene Ontology annotations of the closest human homolog including Gene Ontology terms GO:0002376 (immune system process), GO:0006952 (defense response), and/or GO:0006955 (immune response) as of summer 2021[246].
- the proportion of housekeeping genes defined as genes with stable expression across many human tissues, listed in Eisenberg & Levanon[247].
- the overall dN/dS ratio estimated by Busted for the orthologous CDS alignments.

We match the overall dN/dS between VIPs and control non-VIPs to account for an important issue of dN/dS tests: dN/dS-based tests tend to lose statistical power to detect positive selection in CDS alignments with higher selective constraint[248]. The amount of positively selected sites being equal, positive selection tests based on dN/dS tend to have lower statistical power and tend to generate more false negative results when the rest of the coding sequence is more highly constrained. VIPs tend to be much more strongly constrained than non-VIPs[112], which gives a strong, unfair statistical disadvantage to VIPs when testing positive selection with BUSTED or other HYPHY tests. We limit this issue by matching VIPs and control non-VIPs for dN/dS. Thus, VIPs have an excess of adaptation compared to non-VIPs when they have a balance of the same total amount of non-synonymous changes more tilted towards advantageous rather than neutral amino acid changes. In this case non-VIPs still have less constraint (more neutral changes) than VIPs, and thus still more power to detect positive selection, but not to an extent as severe and unfair as if we did not match the overall dN/dS[112]. In the case where VIPs do not have an excess of adaptation, then they have the same balance of advantageous and neutral amino acid changes resulting in the same overall dN/dS. This is the case of RNA VIPs in bats in this study; this internal negative control shows that the matching of dN/dS works as intended.

Gene Duplications

To quantify patterns of gene duplication and loss, we quantified the copy number of genes with human orthologs from our gene annotations for each nearctic *Myotis* genome. To calculate per-gene expansion and loss rates and their statistical significance, we ran CAFE[140] v5 on the previously described set of copy number counts using our time-calibrated species tree pruned to include only the nine nearctic *Myotis* species. *M. myotis* was excluded because of its lower quality assembly. We ran CAFE on the subset of genes with two or more copies in at least one species using a Poisson distribution for the root frequency (*-p*), first generating an error model to correct for genome assembly and annotation error (*-e*). We compared the base model (each gene family belongs to the same evolutionary rate category) to gamma models (each gene family can belong to one of *k* evolutionary rate categories) with different values of *k*. A final gamma model with *k*=9 was chosen to balance model log likelihood with the number of gene families for which the optimizer failed. The model was run three separate times to ensure convergence.

To understand if genes in these pathways have higher birth rates or are more likely to have significant changes in gene copy number than expected relative to other genes, we compared the gene copy birth rate λ and number of genes that have significantly expanded or contracted in copy number on at least one branch within our nearctic *Myotis* phylogeny. Following Huang et al.[50], we tested if VIP genes in particular underwent

significant copy number changes or had significantly different birth/death rates than non-VIP genes. For each category of VIP genes (all VIPs, DNA VIPs, DNA only VIPs, RNA VIPs, and RNA only VIPs), we generated 100 bootstrap sets of control non-VIP genes with the same number of genes as the corresponding VIP gene set. We ran CAFE on each set of VIP genes and the corresponding control non-VIP genes to infer per-gene birth-death rates and per-gene, per-branch expansion/loss events.

Assessment of DNA Double-Strand Break Tolerance

We assessed each species' tolerance to DNA double strand breaks using a by measuring viability, cytotoxicty, and apoptosis across a range of doses of Neocarzinostatin, a radiomimetic drug. We measured dose response curves in wing-derived primary dermal fibroblasts across 5 bat species (*Myotis lucifugus*, n=8; *Myotis evotis*, n=3; *Rousettus langosus*, n=2; *Eidolon helvum*, n=2; *Pteropus rodrigensis*, n=2) using the multiplexed ApoTox-Glo assay (Promega). Using 96-well plates, two individuals and 11 doses were assessed simultaneously with four technical replicates. Results were normalized to treatment controls for each individual in R as previously described[44,45,48,51].

Mapping PKR exons

We further validated the annotations for the PKR locus by re-aligning the primary *M. velifer* coding sequence back to the nine nearctic *Myotis* reference genomes, as well as a non-*Myotis* outgroup, *Pipistrellus pygmaeus*, and the genome haplotypes for each of these species. Because the presence of two copies makes this task challenging for most aligners, we independently aligned the *M. velifer* reference PKR sequence to sequential sections of each genome in 50kb search regions surrounding the known loci in each genome. This alignment search was conducted for 5 regions upstream (250 kb) and 5 regions downstream (250 kb) of the known loci. In species with two known copies, the location of each copy was included in a separate search region. This was to prevent erroneous merging or loss of exons. These regions were retrieved using bedtools getfasta[249] and alignment was performed using miniprot[62]. Miniprot settings were optimized to retain secondary alignments (-p 0 -n 1 –outsc=0.0 –outc=0.0) and find known exons with accurate boundaries (-J 18 -F 21 -O 15 -L 10). The resulting gff file was converted to bed format using AGAT[250], sequences retrieved with bedtools getfasta, and a custom script used to remove identical duplicates. Finally, all sequences were aligned with MACSE v2.07[225]. We used BISER[128,211] to confirm the presence of segmental duplications in these regions.

PKR cell lines and vectors

All PKR experiments were performed using HeLa PKR-KO cells (kindly provided by A. Geballe, Fred Hutchinson Cancer Center, Seattle WA) that were plated either at densities of 5x10^4 cells/mL in 24-well plates or at 1x10^5 cells/mL in 12-well plates. The cells were maintained at 37°C with 5% CO_2 and cultured in DMEM supplemented with 5% fetal bovine serum (FBS), 1% penicillin/ streptomycin mix and 1 µg/mL puromycin (Sigma-Aldrich). All transfections were performed 24 hours after seeding, using 3 µL of TransIT-LT1 Transfection Reagent (Mirus Bio) per 1 µg of DNA and Opti-MEM media. We used previously-generated pSG5-FLAGx2 vectors encoding either *M. myotis* PKR-1 (GenBank OP006550), *M. myotis* PKR-2 (GenBank OP006559), *M. velifer* PKR-1 (GenBank OP006558), or *M. velifer* PKR-2 (GenBank OP006557)[28]. Plasmids encoding the interferon-stimulated gene ISG20[243] and a constitutively active variant of the sterile alpha motif domain-containing protein 9-like SAMD9L-F886Lfs*11 (here, SAMD9L[251]) were used as controls in viral infections and cell translation experiments, respectively.

Western blot

We assessed for the steady state protein expression of *M. myotis* Flag-PKRs after transfection of 350 ng and 700 ng of DNA plasmids encoding either PKR1 alone, PKR2 alone, or both PKR1 and PKR2 (175 ng of each and 350 ng of each, respectively). Briefly, cells were re-suspended and lysed in ice-cold RIPA buffer (50 mM Tris pH8, 150 mM NaCl, 2 mM EDTA, 0.5% NP40) with protease inhibitor cocktail (Roche) and sonicated. 20 µL of the clarified fraction was denatured with 5 µL of 6x Laemmli buffer at 95°C for 5 min and loaded into 4-20% BioRad Criterion TGX Stain-Free precast gel. The wet transfer into a PVDF membrane was executed overnight at 4°C. The membranes were blocked in a 1xTBS-T buffer (Tris HCl 50 mM pH8, NaCl 30 mM, 0.05% of Tween 20) containing 10 % powder milk, and were incubated for 1h. The membranes were incubated with primary mouse anti-Flag (Sigma F3165) and anti-Tubulin (Sigma T5168) antibodies and secondary anti-Mouse IgG-Peroxidase conjugated (Sigma A9044). Detection was made using the Chemidoc Imagina System (BioRad) with SuperSignal West Pico Chemiluminescent Substrate (ThermoFisher Scientific).

Cell viability assay

Hela PKR-KO cells were transfected 24h after plating in 96 well plates, with 100 or 200 ng of pSG5 plasmid: empty or coding for *M. myotis* or *M. velifer* PKR1, PKR2 or PKR1+2 equal mix (50%-50%). 24 hours post-transfection, positive control cells were treated with an apoptosis-inducing drug, Etoposide, at different doses (250, 200 or 100 µM). 48 hours post transfection, cells were harvested and lysed to quantify luminescent signal according to CellTiter-Glo® Luminescent Cell Viability Assay (Promega) kit protocol.

VSV infection

Cells were transfected 24 h after plating with 350 ng of pSG5 plasmid: empty, or encoding *M. myotis* or *M. velifer* PKR1, PKR2, or equal input of PKR1 and PKR2 (175 ng per plasmid), or a plasmid encoding interferon-stimulated exonuclease gene 20 (ISG20), due to its known antiviral activity against VSV as positive control[243]. Cells were infected 24 h post transfection with replicative VSV-GFP virus[145] at a MOI of 3. Cells were fixed with 4% paraformaldehyde 16-18 hours post infection. VSV infection was quantified by measuring the percentage of GFP positive cell populations with BD FACSCanto II Flow Cytometer (SFR BioSciences). Fold change results were normalized to the empty pSG5 condition across at least three independent experiments.

Luciferase reporter assays

Luciferase reporter assays were carried out to investigate whether the two PKR paralogs have synergistic, additive or dominant negative effect in translation shutdown. Transfection was performed as previously described with additional 50 ng of FFLuc firefly luciferase reporter plasmid per well. Sterile alpha motif domain-containing proteins 9L (SAMD9L gain-of-function mutant) was used as a positive control of translational repression[251]. 24 h post transfection, cells were briefly washed with PBS, lysed by a 5× reporter lysis buffer (Promega) and incubated overnight at -20°C. Cells were then collected and 100 µl of the luciferase substrate (Promega) was added to 20 µl of the lysis supernatant. Alternatively, cells were lysed using BrightGlow Lysis Reagent (Promega E2620). The relative luminescence units (RLUs) were immediately quantified with LUMIstar

Omega microplate reader optima (BMG Labtech). All luciferase assays were conducted in technical duplicates in at least five independent experiments. Fold change results were normalized to the empty pSG5 condition within each independent experiment.

Figures

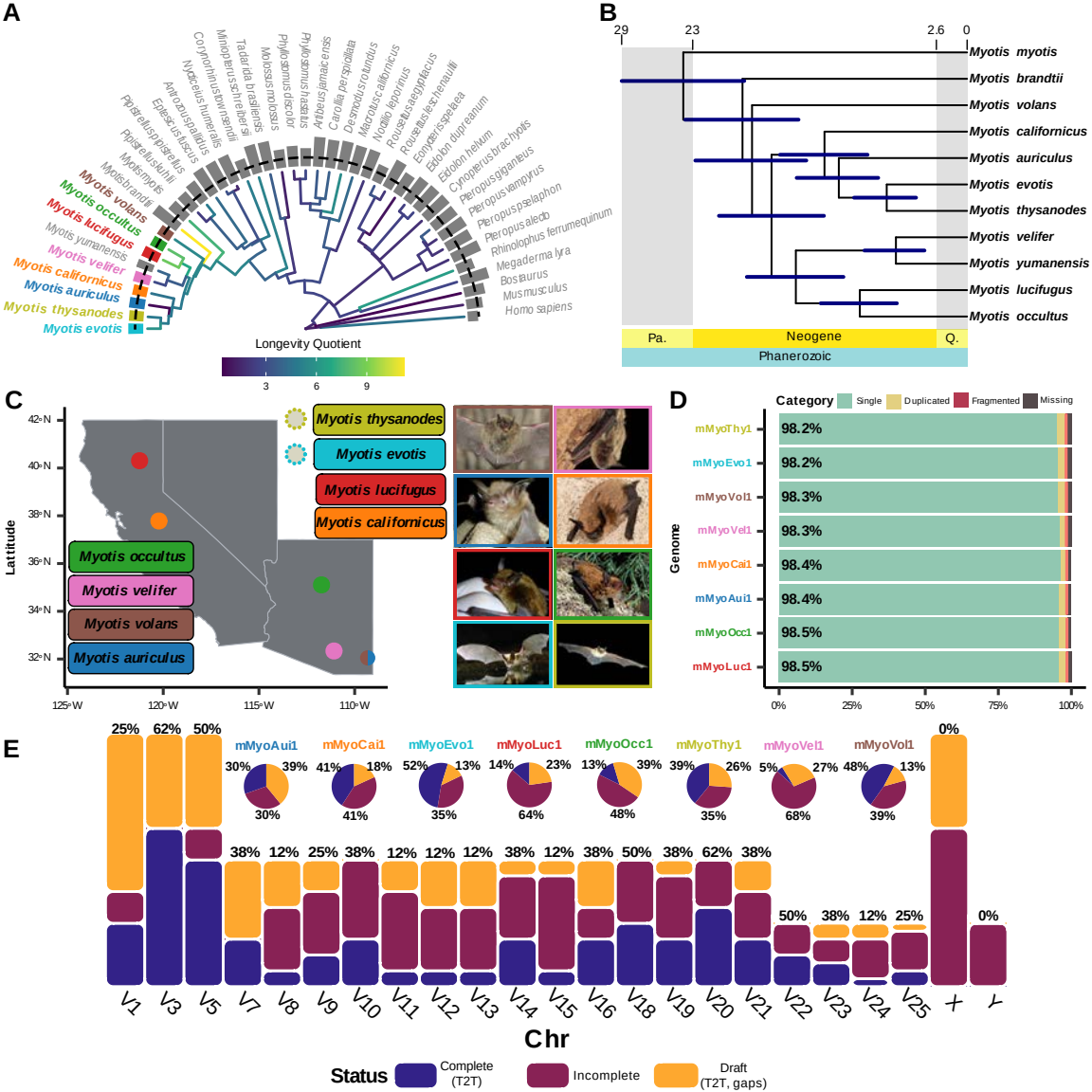
A
Longevity Quotient
3
6
9
Myotis volans
Myotis lucifugus
Myotis yumanensis
Myotis velifer
Myotis californicus
Myotis auriculus
Myotis thysanodes
Myotis evotis
Homo sapiens
B
29
23
2.6
0
Myotis myotis
Myotis brandtii
Myotis volans
Myotis californicus
Myotis auriculus
Myotis evotis
Myotis thysanodes
Myotis velifer
Myotis yumanensis
Myotis lucifugus
Myotis occultus
Pa.
Neogene
Q.
Phanerozoic
C
Myotis thysanodes
Myotis evotis
Myotis lucifugus
Myotis californicus
Myotis occultus
Myotis velifer
Myotis volans
Myotis auriculus
Latitude
42°N
40°N
38°N
36°N
34°N
32°N
125°W
120°W
115°W
110°W
D
Category
Single
Duplicated
Fragmented
Missing
Genome
mMyoThy1 98.2%
mMyoEvo1 98.2%
mMyoVol1 98.3%
mMyoVel1 98.3%
mMyoCai1 98.4%
mMyoAui1 98.4%
mMyoOcc1 98.5%
mMyoLuc1 98.5%
0%
25%
50%
75%
100%
E
mMyoAui1 30% 39% 30%
mMyoCai1 41% 18% 41%
mMyoEvo1 52% 13% 35%
mMyoLuc1 14% 23% 64%
mMyoOcc1 13% 39% 48%
mMyoThy1 39% 26% 35%
mMyoVel1 5% 27% 68%
mMyoVol1 48% 13% 39%
25% 62% 50% 38% 12% 25% 38% 12% 12% 12% 38% 12% 38% 50% 38% 62% 38% 50% 38% 12% 25% 0% 0%
V1 V3 V5 V7 V8 V9 V10 V11 V12 V13 V14 V15 V16 V18 V19 V20 V21 V22 V23 V24 V25 X Y
Chr
Status
Complete (T2T)
Incomplete
Draft (T2T, gaps)

Figure 1: 8 near-complete reference assemblies for North American (Nearctic) *Myotis*. **A)** Phylogeny of 38 bat genomes with 3 outgroup species: cow *(bosTau9*), mouse (*mm39*); and human (*T2T-CHM13v2.0*). Bars at the tips of the phylogeny indicate the AuNG score of each genome (lower values equal more contiguous genomes); the dotted line represents the AuNG score for complete (T2T) genome assemblies as represented by T2T-CHM13v2.0. **B)** The time-calibrated phylogeny of 9 Nearctic and two representative Palaearctic *Myotis* species based on orthologous codon alignments. Blue bars represent age uncertainties. **C)** Map of capture sites with representative images (see "Acknowledgements" for attributions) for the individuals and species sequenced in this study; cell lines for *M. evotis* and *M. thysanodes* were provided by Richard Miller and were not collected for this study. **D)** BUSCO (v5, odb10_mammalia) scores for annotations generated for the 8 new *Myotis* genomes. **E)** Ideogram bar plot indicating completion status of each chromosome in assembly. Pie graphs indicate completion status of all chromosomes in assembly. All chromosomes were positively identified based on size, synteny, and homology to human chromosomes[57]. "Complete (T2T)" status indicates that a chromosome is fully assembled telomere-to-telomere without gaps; "Draft (T2T, gaps)" status indicates that a chromosome is fully scaffolded with both telomeres, but has one or more gaps in the assembly; "Incomplete" status indicates that a chromosome was positively identified, but was not scaffolded from telomere to telomere (only contains one telomere).

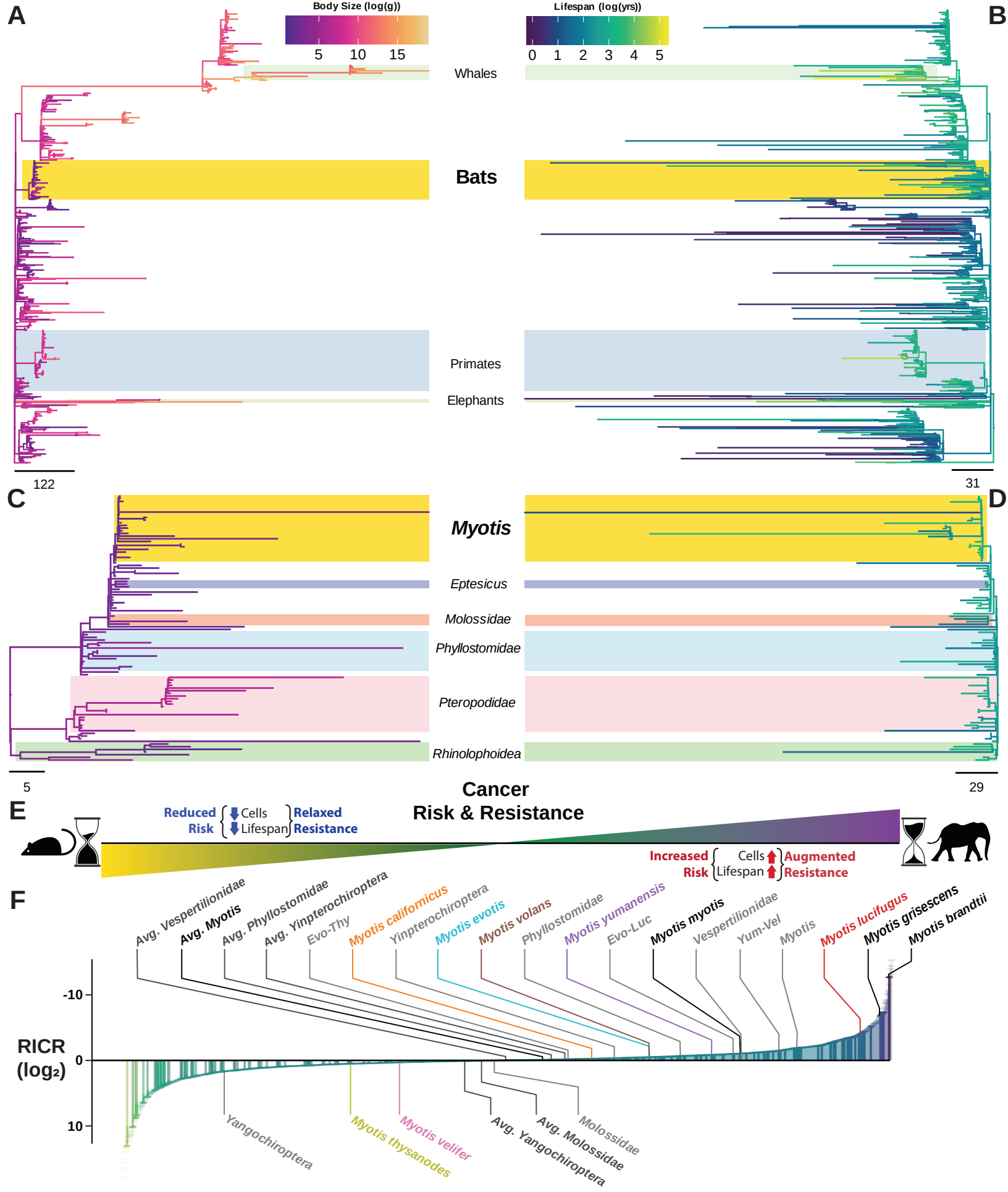
A
Body Size (log(g))
5
10
15
B
Lifespan (log(yrs))
0
1
2
3
4
5
Whales
Bats
Primates
Elephants
122
31
C
D
Myotis
Eptesicus
Molossidae
Phyllostomidae
Pteropodidae
Rhinolophoidea
5
29
Cancer
Risk & Resistance
E
Reduced Risk
Cells
Lifespan
Relaxed Resistance
Increased Risk
Cells
Lifespan
Augmented Resistance
F
Avg. Vespertilionidae
Avg. Myotis
Avg. Phyllostomidae
Avg. Yinpterochiroptera
Evo-Thy
Myotis californicus
Yinpterochiroptera
Myotis evotis
Myotis volans
Phyllostomidae
Myotis yumanensis
Evo-Luc
Myotis myotis
Vespertilionidae
Yum-Vel
Myotis
Myotis lucifugus
Myotis grisescens
Myotis brandtii
RICR
(log2)
-10
0
10
Yangochiroptera
Myotis thysanodes
Myotis velifer
Avg. Yangochiroptera
Avg. Molossidae
Molossidae

Figure 2: Evolution of body size, lifespan, and cancer risk in bats and mammals. **A, B)** Cophylo plot of the evolution of body size (**A**) and lifespan (**B**) across *Eutheria*. **C, D)** Cophylo plot of the evolution of body size (**C**) and lifespan (**D**) in bats. Branch lengths in **A-D** are scaled proportional to the rate of change of the trait over time, and tree scales are shown below their respective phylogenies. **E)** Diagram illustrating the relationship between changes in body size and lifespan with changes in cancer risk and resistance. Changes in either body size or lifespan are directly proportional to changes in theoretical cancer risk; to resolve Peto's Paradox and normalize cancer risk across mammals[89,92], changes in theoretical cancer risk must be inversely proportional to changes of the intrinsic cancer risk per cell, implying increased cancer resistance. **F)** Reduced Intrinsic Cancer Risk (RICR) for every node in *Eutheria*, ranked from greatest reduction in cancer risk to greatest increase in cancer risk. RICR relative to the most recent ancestor of select nodes are highlighted, as well as the average RICR across for all nodes within select clades.

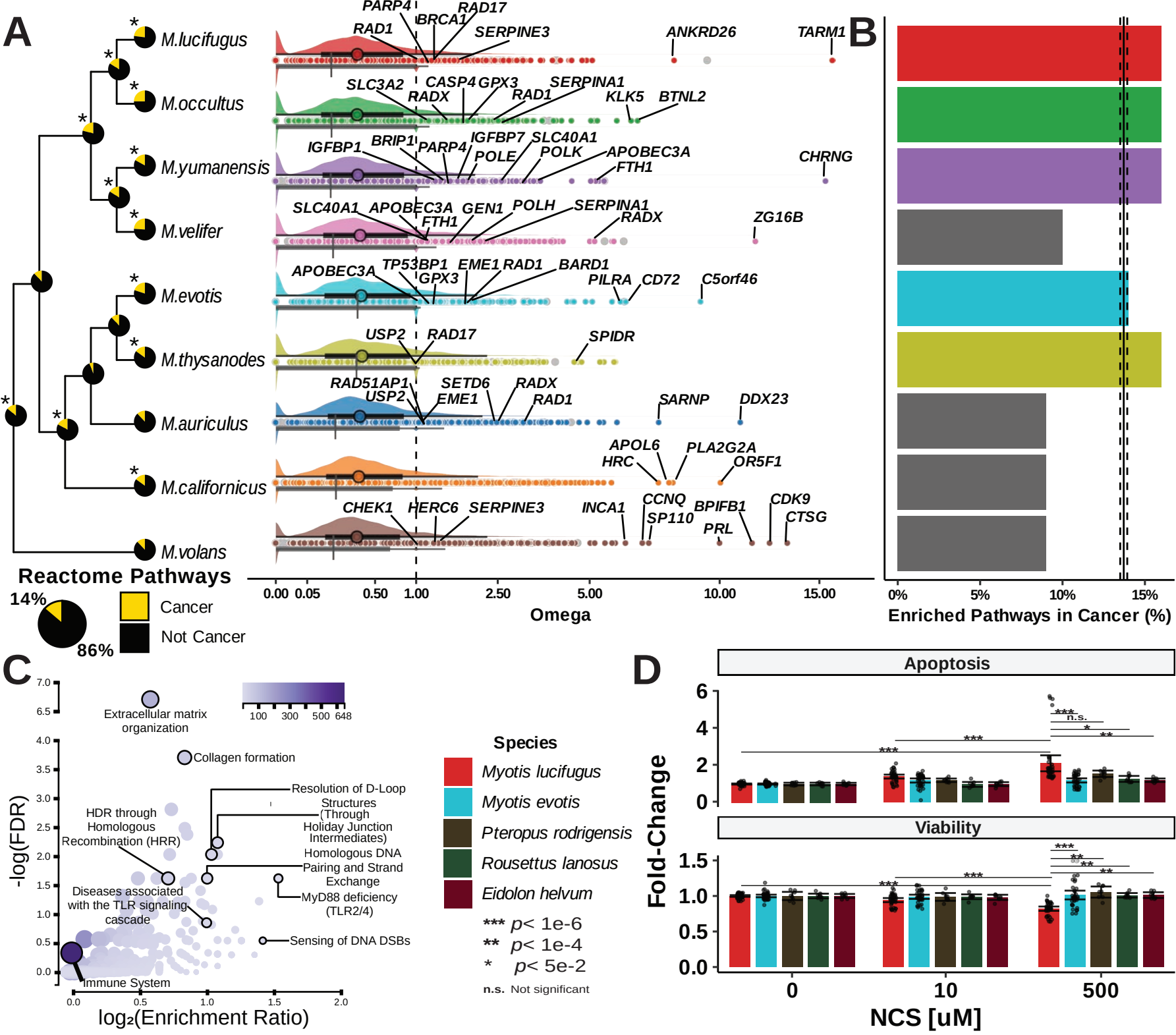
A
M.lucifugus
M.occultus
M.yumanensis
M.velifer
M.evotis
M.thysanodes
M.auriculus
M.californicus
M.volans
PARP4
BRCA1
RAD17
RAD1
SERPINE3
ANKRD26
TARM1
SLC3A2
CASP4
GPX3
SERPINA1
RADX
RAD1
KLK5
BTNL2
IGFBP1
BRIP1
PARP4
IGFBP7
SLC40A1
POLE
POLK
APOBEC3A
FTH1
CHRNG
SLC40A1
APOBEC3A
GEN1
POLH
SERPINA1
FTH1
RADX
ZG16B
APOBEC3A
TP53BP1
EME1
RAD1
BARD1
GPX3
PILRA
CD72
C5orf46
USP2
RAD17
SPIDR
RAD51AP1
SETD6
RADX
USP2
EME1
RAD1
SARNP
DDX23
APOL6
PLA2G2A
HRC
OR5F1
CHEK1
HERC6
SERPINE3
INCA1
CCNQ
BPIFB1
CDK9
SP110
CTSG
PRL
0.00 0.05 0.50 1.00 2.50 5.00 10.00 15.00
Omega
Reactome Pathways
14%
86%
Cancer
Not Cancer
B
0% 5% 10% 15%
Enriched Pathways in Cancer (%)
C
Extracellular matrix organization
Collagen formation
Resolution of D-Loop Structures (Through Holiday Junction Intermediates)
HDR through Homologous Recombination (HRR)
Homologous DNA Pairing and Strand Exchange
Diseases associated with the TLR signaling cascade
MyD88 deficiency (TLR2/4)
Sensing of DNA DSBs
Immune System
-log(FDR)
log2(Enrichment Ratio)
100 300 500 648
Species
Myotis lucifugus
Myotis evotis
Pteropus rodrigensis
Rousettus lanosus
Eidolon helvum
*** p< 1e-6
** p< 1e-4
* p< 5e-2
n.s. Not significant
D
Apoptosis
Viability
Fold-Change
0 10 500
NCS [uM]

Figure 3: Selection in Nearctic *Myotis* is enriched for pleiotropic cancer resistance pathways. **A) Left**: phylogeny of Nearctic *Myotis*; **Right**: raincloud plot of omega values for all genes in each species since its most recent ancestor. The distribution of omega (**ω**) values for significant ($p \leq 0.05$ after multiple testing correction) genes and all genes is shown in color above the line. The 95% confidence interval and median for significant **ω**'s are represented by the black bar and circle, respectively; the overall 95% confidence interval and median are shown in grey below. Individual genes' **ω**'s are represented by colored points. Individual genes' omega values and grey, respectively. **Left inset**: Proportion of cancer-associated Reactome pathways among the top 100 pathways overrepresented among genes under selection at each node. Below, pie chart indicates expected proportion of pathways out of 100 that are cancer-associated after 1000 random samples. Nodes with proportions greater than the expected value with $p \leq 0.05$ using Fisher's exact test are indicated with an asterisk. **B)** Proportion of cancer-associated Reactome pathways among the top 100 pathways overrepresented among genes under selection across all nodes in a species' evolutionary history. **C)** Volcano plot of overrepresented pathways in Reactome among the union set of genes under selection across all nodes in the evolutionary history for *M. lucifugus*. **D)** Viability and Apoptosis fold-change in 5 bat species in response to different doses of neocarzinostatin, a potent inducer of DNA double-strand breaks. Points represent individual replicates normalized to each species' control, while bars represent mean ± 95% confidence intervals.

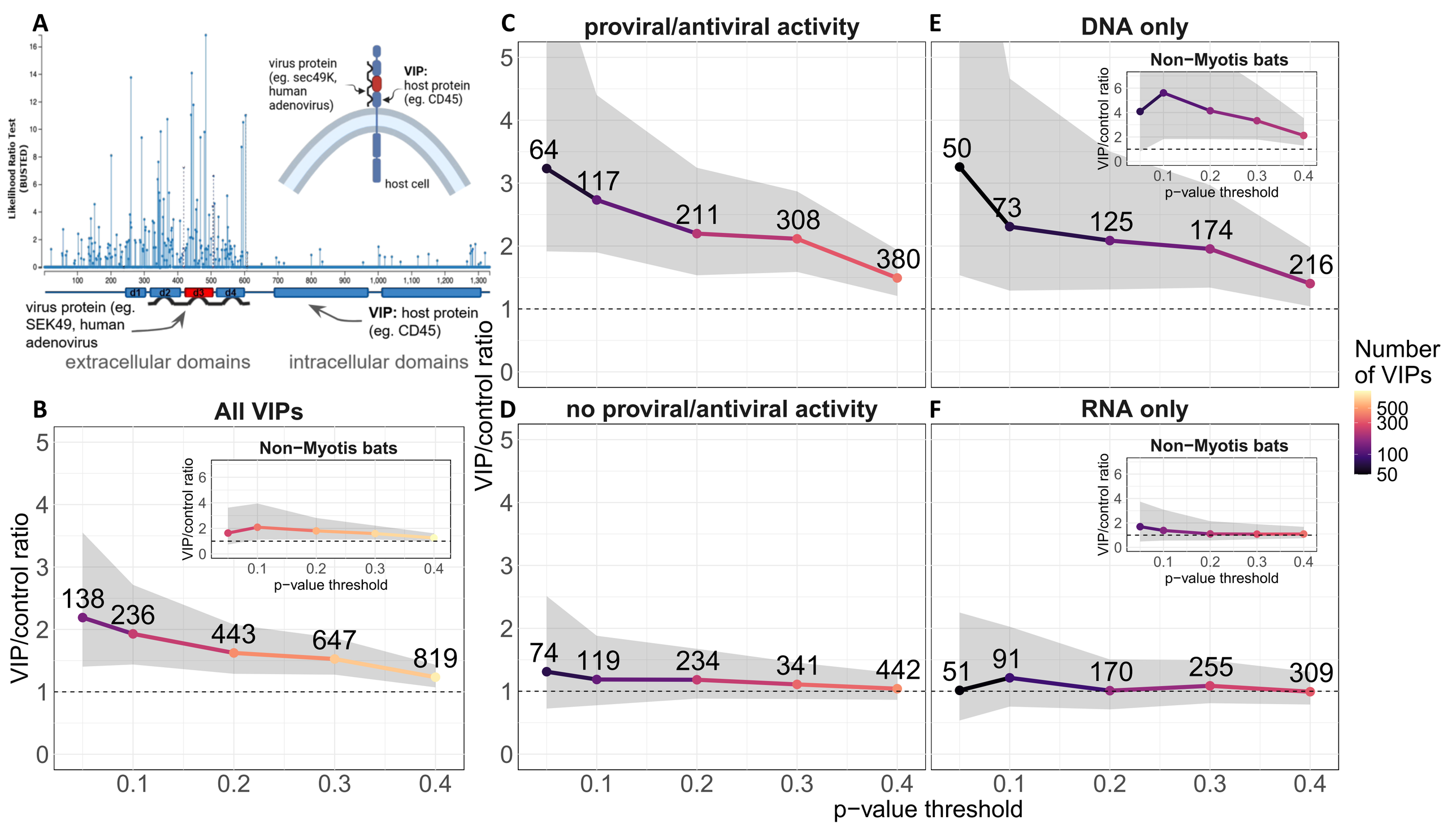
A
Likelihood Ratio Test (BUSTED)
virus protein (eg. sec49K, human adenovirus)
VIP: host protein (eg. CD45)
host cell
d1
d2
d3
d4
virus protein (eg. SEK49, human adenovirus
VIP: host protein (eg. CD45)
extracellular domains
intracellular domains
B
All VIPs
Non−Myotis bats
VIP/control ratio
p−value threshold
138
236
443
647
819
C
proviral/antiviral activity
64
117
211
308
380
D
no proviral/antiviral activity
74
119
234
341
442
E
DNA only
50
73
125
174
216
F
RNA only
51
91
170
255
309
Number of VIPs
500
300
100
50

Figure 4: Adaptation to DNA viruses, but not RNA viruses, is enriched in *Myotis* and other bats. **A)** Diagram of an example VIP, CD45: a host cell transmembrane receptor that interacts with the human adenovirus protein sec49K. Previous work has shown that the amino acids of CD45 that participate in this direct interaction are under strong positive selection, as indicated in the graph above the cartoon. **B-F)** Enrichment plots showing the ratio of positive selection in VIPs versus matched sets of control genes at different p-value thresholds. The solid line shows the median ratio; the color of the line, and the number above each point, represents the number of VIPs with significant BUSTED-MH p-values at the given threshold; the grey band represents the 95% confidence interval generated by bootstrapping sets of matched control genes. Inset plots show the same for all bats in this study excluding *Myotis*.

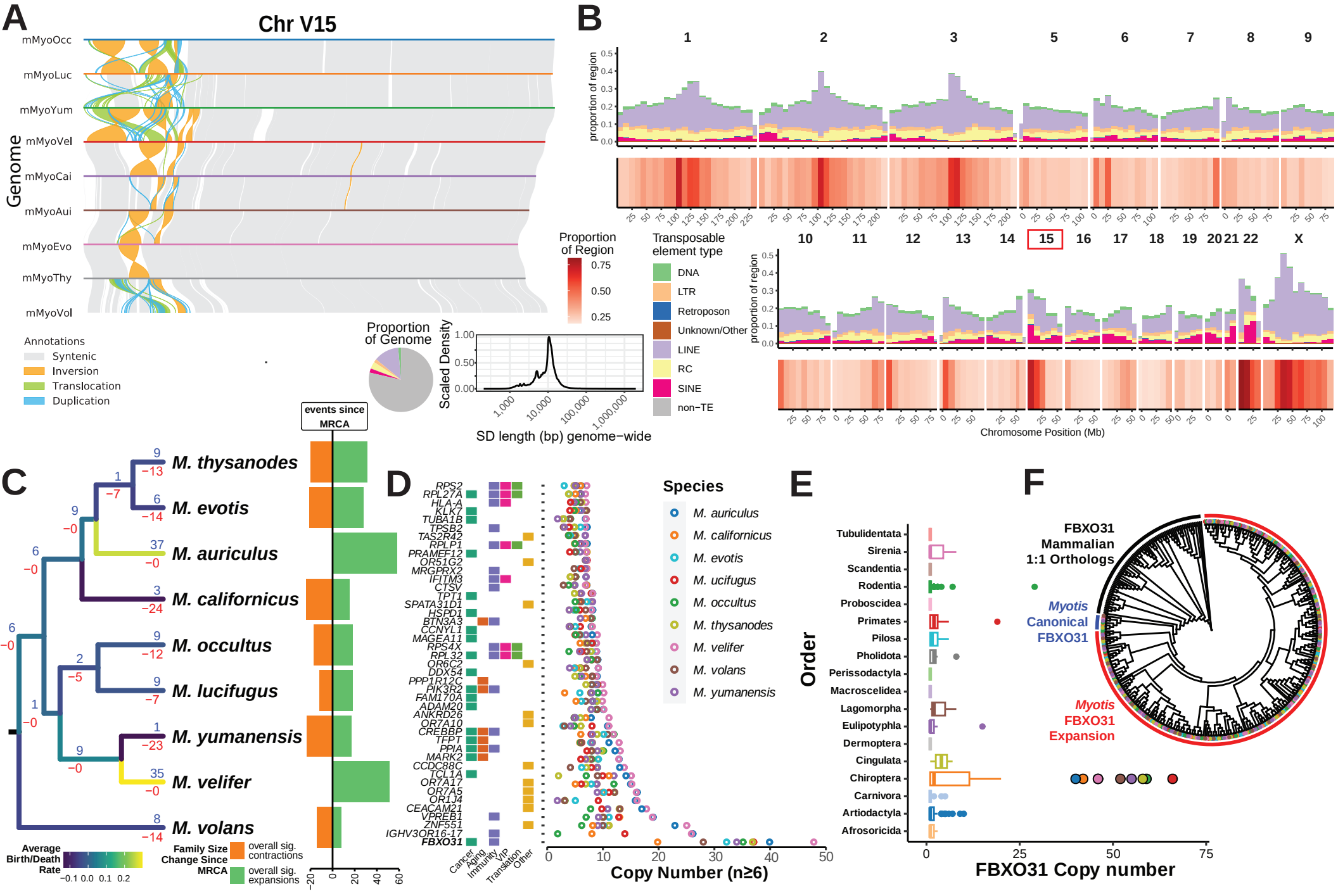
A
Chr V15
Genome
mMyoOcc
mMyoLuc
mMyoYum
mMyoVel
mMyoCai
mMyoAui
mMyoEvo
mMyoThy
mMyoVol
Annotations
Syntenic
Inversion
Translocation
Duplication
B
proportion of region
Proportion of Region
Transposable element type
DNA
LTR
Retroposon
Unknown/Other
LINE
RC
SINE
non−TE
Proportion of Genome
Scaled Density
SD length (bp) genome−wide
Chromosome Position (Mb)
C
M. thysanodes
M. evotis
M. auriculus
M. californicus
M. occultus
M. lucifugus
M. yumanensis
M. velifer
M. volans
events since MRCA
Average Birth/Death Rate
Family Size Change Since MRCA
overall sig. contractions
overall sig. expansions
D
Species
M. auriculus
M. californicus
M. evotis
M. ucifugus
M. occultus
M. thysanodes
M. velifer
M. volans
M. yumanensis
Cancer
Aging
Immunity
VIP
Translation
Other
Copy Number (n≥6)
E
Order
Tubulidentata
Sirenia
Scandentia
Rodentia
Proboscidea
Primates
Pilosa
Pholidota
Perissodactyla
Macroscelidea
Lagomorpha
Eulipotyphla
Dermoptera
Cingulata
Chiroptera
Carnivora
Artiodactyla
Afrosoricida
FBXO31 Copy number
F
FBXO31 Mammalian 1:1 Orthologs
Myotis Canonical FBXO31
Myotis FBXO31 Expansion

Figure 5: A varied structural variation landscape across 9 nearctic *Myotis* species. **A)** Synteny between *Myotis* species on chromosome V15, showing syntenic regions (grey), inversions (orange), translocations (green), and duplications (blue). Regions with high proportions of telomeric repeats were masked prior to alignment. **B)** Distribution of transposable elements and segmental duplicates in mMyoVel1. Pie chart indicates overall genome proportions of TEs; histogram represents the size distribution of segmental duplications genome-wide. **C)** CAFE results among our Nearctic *Myotis* relative to single-copy human orthologs. Phylogeny is colored by the estimated birth/death rate (λ) for all genes examined. Bar plot indicates the cumulative number of significant gain and loss events for each species. **D)** Per-genome copy numbers of all genes with over 6 copies in any Nearctic *Myotis* genome. Genes are classified into 5 categories (cancer, aging, immunity, VIP, translation, and "Other") based on literature reviews on PubMed. **E)** Copy number estimates of *FBXO31* across 536 mammalian genomes identified using Reciprocal Best-Hit BLAT. **F**) Gene-tree reconciliation of FBXO31 across mammals generated using GeneRax.

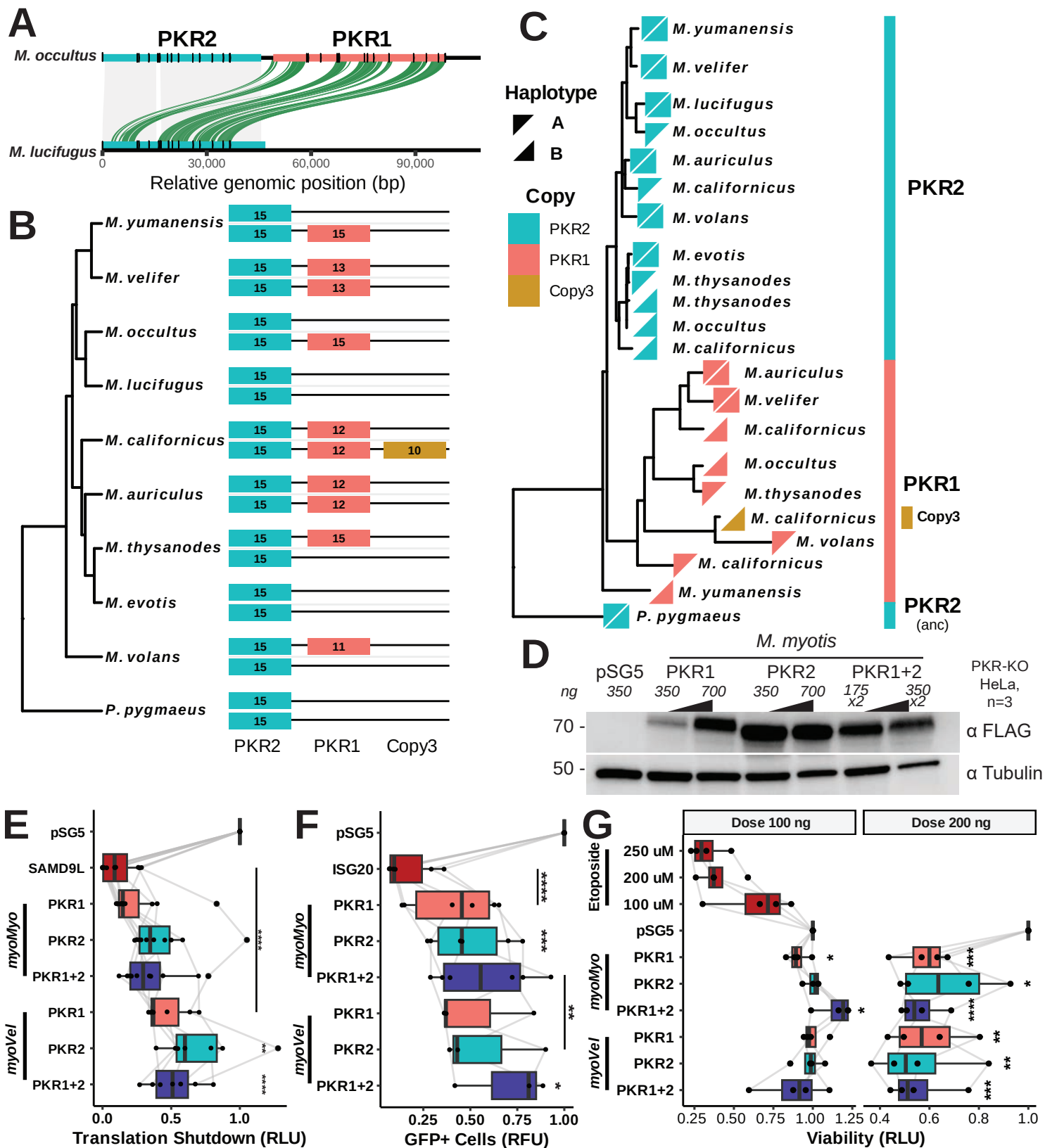
A
PKR2
PKR1
M. occultus
M. lucifugus
0
30,000
60,000
90,000
Relative genomic position (bp)
B
M. yumanensis
M. velifer
M. occultus
M. lucifugus
M. californicus
M. auriculus
M. thysanodes
M. evotis
M. volans
P. pygmaeus
PKR2
PKR1
Copy3
C
Haplotype
A
B
Copy
PKR2
PKR1
Copy3
M. yumanensis
M. velifer
M. lucifugus
M. occultus
M. auriculus
M. californicus
M. volans
M. evotis
M. thysanodes
M. thysanodes
M. occultus
M. californicus
M. auriculus
M. velifer
M. californicus
M. occultus
M. thysanodes
M. californicus
M. volans
M. californicus
M. yumanensis
P. pygmaeus
PKR2
PKR1
Copy3
PKR2
(anc)
D
M. myotis
pSG5
PKR1
PKR2
PKR1+2
ng
350
350
700
350
700
175 x2
350 x2
PKR-KO HeLa, n=3
70 -
50 -
α FLAG
α Tubulin
E
pSG5
SAMD9L
PKR1
PKR2
PKR1+2
PKR1
PKR2
PKR1+2
myoMyo
myoVel
Translation Shutdown (RLU)
F
pSG5
ISG20
PKR1
PKR2
PKR1+2
PKR1
PKR2
PKR1+2
myoMyo
myoVel
GFP+ Cells (RFU)
G
Dose 100 ng
Dose 200 ng
Etoposide
250 uM
200 uM
100 uM
pSG5
PKR1
PKR2
PKR1+2
PKR1
PKR2
PKR1+2
myoMyo
myoVel
Viability (RLU)

Figure 6: Evolutionary history and function of an actively segregating copy number polymorphism of *PKR* in *Myotis*. **A)** Structural comparison of the single- and dual-copy PKR haplotypes across two species. Orthologous regions between the two haplotypes are indicated by grey bands, while syntenic duplications are indicated in green. Exons in *PKR1* and *PKR2* are annotated with black marks. **B)** Cartoon of the PKR locus in the two phased haplotype assemblies of each species. While *PKR2* is present across all haplotypes, *PKR1* and PKR copy 3 are polymorphic within and across species. Each number indicates the number of exons identified for each gene in the haplotype. **C)** The reconciled gene tree for all copies of *PKR* across all haplotypes and species shown in **B.** The haplotype corresponding to the reference genome of each species (haplotype A) is represented by an upper-diagonal triangle, while the alternative haplotype (haplotype B) is represented by a lower-diagonal triangle. Nodes where both copies of a gene were sister to one another were collapsed into a single rectangle for clarity. **D)** Steady state protein expression levels in $PKR^{-/-}$ HeLa cells transfected with plasmids encoding FLAG-tagged *Myotis myotis* PKR1 and PKR2 plasmids. Western blots targeting FLAG or Tublin (loading control) in lysate of cells transfected with increasing amounts of either empty vector (pSG5), *PKR1*-FLAG, *PKR2*-FLAG, or an equimass mix of both PKR vectors. **E)** The effect of *Myotis* PKR copy number on the translation of luciferase, measured in Relative Light Units (RLU) and normalized to the empty vector control. Co-expression of both PKR1 and PKR2 has an additive effect on cell translation shutdown, with no synergy or dominant negative effects observed. Human SAMD9L-GoF was used as a positive control of cell translation inhibition[251]. **F)** The effect of *Myotis* PKR copy number on viral VSV infectivity. The percentage of VSV-GFP infected cells was measured by flow cytometry and normalized to the control pSG5 condition. Although all *Myotis* PKR conditions restrict VSV infection, expressing both PKR1 and PKR2 is not beneficial against VSV infection. ISG20 was used as a positive control of VSV-GFP restriction[243]. **G)** The effect of *Myotis* PKR copy number on cell viability, normalized to the empty vector control. While no effect on viability was observed at a lower total dose of plasmid, at higher doses of PKR there is a significant reduction in cellular viability. Etoposide at 3 doses (100 uM, 200 uM, and 250 uM) were used as a positive control for cell death. For **E-F**, error bars indicate the means ± SEM for at least three independent experiments. Statistical significance was assessed by unpaired t-test of each condition versus control.

Supplemental Information

Document S1. Figures S1-S6
Table S1. Genome Statistics
Table S2. Phylogeny time calibration and evolutionary modeling data
Table S3. aBSREL significant gene lists and Reactome enrichments
Table S4. RERConverge and RELAX results and enrichments
Table S5. List of VIPs and VIP subclasses
Table S6. SyRI-identified structural variants (SVs)
Table S7. Experimental data for Neocarzinostatin and PKR experiments